AD-A065 581 NATIONAL AERONAUTICAL ESTABLISHMENT OTTAWA (ONTARIO) F/G 20/4
CALCULATION OF THE POTENTIAL FLOW PAST MULTI-COMPONENT AIRFOILS--ETC(U)
NOV 78 M MOKRY

UNCLASSIFIED NAE-LR-596 NRC-17246 NL

END
DATE FILMED
5-79
DDC

National Research Council Canada
Conseil national de recherches Canada

LEVEL II

CALCULATION OF THE POTENTIAL FLOW PAST MULTI-COMPONENT AIRFOILS USING A VORTEX PANEL METHOD IN THE COMPLEX PLANE

by
M. Mokry
National Aeronautical Establishment

OTTAWA
NOVEMBER 1978

NRC NO. 17246

AERONAUTICAL REPORT
LR-596

(6)

(6)

CALCULATION OF THE POTENTIAL FLOW PAST MULTI-COMPONENT AIRFOILS USING A VORTEX PANEL METHOD IN THE COMPLEX PLANE

(ÇALCUL DANS LE PLAN COMPLEXE DE L'ÉCOULEMENT À POTENTIEL AUTOUR DE PROFILS À COMPOSANTS MULTIPLES PAR LA MÉTHODE DES PETITS PAVÉS À TOURBILLONS)

(14) NAE-LR-596

by/par

(19) M. MOKRY

(18) NRC
(19) 17246

(11) NOV 78
(12) 50 p.

240300
RLH

L.H. Ohman, Head/Chef
High Speed Aerodynamics Laboratory/
Laboratoire d'aérodynamique à hautes vitesses

F.R. Thurston
Director/Directeur

SUMMARY

An efficient algorithm for a vortex panel method in the complex plane is developed to compute the potential flow past multi-component airfoils in free air and a porous-wall wind tunnel. The theoretical foundations of the method — the properties of the source and vortex density functions, the relationship between the exterior and interior flows, and the general Kutta-Joukowski condition for a trailing edge with crossflow — are derived from the theory of the Cauchy type integral. The method utilizes flat panels with linear vortex and source densities, the latter being used to simulate the displacement effect of boundary layers. The airfoil boundary condition is satisfied at all panel midpoints and the overdetermined system of linear algebraic equations solved as a least squares problem, in the L_1 norm, or in the L_∞ norm. The wind tunnel wall interference problem is treated using the concept of the Green's function in the complex plane. Examples are worked out for some theoretical airfoils and extensive tables of exact and computed pressure distributions are given.

RÉSUMÉ

Le présent ouvrage porte sur la mise au point d'un algorithme efficace qui permettrait de calculer dans le plan complexe, à partir de la méthode des petits pavés à tourbillons, l'écoulement à potentiel autour des profils à composants multiples dans l'air libre et dans une soufflerie à paroi perméable. Les fondements théoriques de la méthode — les propriétés des fonctions de densité des tourbillons et des sources, les relations entre l'écoulement extérieur et intérieur et la condition générale de Kutta-Joukowski pour un bord de fuite avec écoulement transversal — sont tirés de la théorie de l'intégrale de Cauchy. La méthode fait intervenir des pavés plans présentant des fonctions linéaires de densité des tourbillons et des sources, ces dernières permettant de simuler l'effet de déplacement des couches limites. Les conditions aux limites des profils sont satisfaites en tout point médian des pavés, et le système algébrique d'équations linéaires hyperdéterminées est résolu par la méthode des moindres carrés ou de la norme L_1 ou L_∞. L'effet de la paroi de la soufflerie est traité en termes du concept de la fonction de Green dans le plan complexe. Quelques exemples de profils théoriques sont analysés et des tables complètes des valeurs exactes de différentes répartitions de pression sont données.

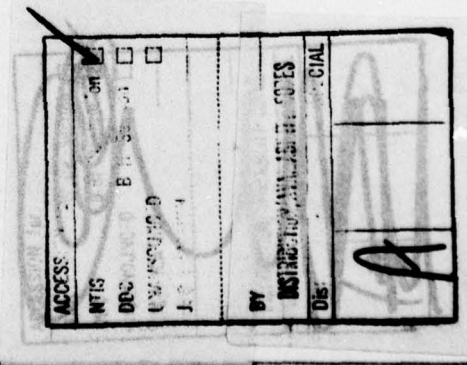

CONTENTS

TABLES

ILLUSTRATIONS

CALCULATION OF THE POTENTIAL FLOW PAST MULTI-COMPONENT AIRFOILS USING A VORTEX PANEL METHOD IN THE COMPLEX PLANE

1.0 INTRODUCTION

The simplicity and compactness of a two-dimensional panel method developed in the complex plane was first demonstrated by Giesing, Reference 1, on flat panels with a constant source density, which are the building stones of the Douglas-Neumann source distribution method. Having in mind a similar approach to a contemporary vortex panel method, which uses linear distributions of source and vortex densities over the panels, the present report outlines first a theory of distributions of sources and vortices in the complex plane. The properties of the source and vortex density functions and the relationship between the exterior and interior flows are derived using the concept of the Cauchy type integral. The novelty of the present approach is that the integral is linked to the complex disturbance velocity and not to the potential function, so that no artificial discontinuity lines need to be introduced in the flow field. The Cauchy type integral is also used to derive the general Kutta-Joukowski condition in terms of the trailing edge values of the source and vortex densities. The connection between the conditions of a finite trailing edge velocity and the geometrical concept of equal upper and lower trailing edge velocities is elucidated upon.

The major part of the work is focussed on the development of an algorithm for a vortex panel method which uses flat panels with linear distributions of source and vortex densities. The corner values of the source density, used to simulate the displacement effect of boundary layers, enter as given quantities and the corner values of the vortex density, determining tangent components of velocity, are the quantities to be solved for. Since the airfoil boundary condition is met at all panel midpoints and the Kutta-Joukowski condition is satisfied at trailing edges, the resultant system of linear algebraic equations is overdetermined and solved by minimizing the residual norm. Because of the compactness of the integration in the complex plane, the elements of the matrix can be given in full for a multi-component airfoil case and the coding of a computer program becomes a relatively simple matter.

The treatment of flow past airfoils under the constraint of wind tunnel walls is based on the concept of Green's function in the complex plane. To a large extent, it is an incorporation of earlier research results, References 2-4, in the vortex panel method. The material is organized in such a way that the method for the calculation of flow past an airfoil in the wind tunnel is presented as a modification of the method developed for an airfoil in free air, and is easy to use to assess the effects of wind tunnel wall interference. Although in the context of the present method the introduction of the concept of the angle of attack is not necessary at all, it was found to be useful in the interpretation of the wind tunnel computations and to show the limitations of conventional wall correction techniques when applied to high lift systems.

2.0 DISTRIBUTION OF SOURCES AND VORTICES

Let D^- be an infinite, connected region in the complex plane bounded by several non-intersecting airfoil contours $L_1, L_2, \ldots L_n$, oriented counterclockwise as shown in Figure 1. By L we denote the union

$$L = \bigcup_{\ell=1}^{n} L_\ell$$

and by D^+ the complement of $D^- \cup L$. The region D^+ thus consists of n simple closed interior regions $D_1^+, D_2^+, \ldots, D_n^+$ bounded by the contours $L_1, L_2, \ldots L_n$.

Consider the Cauchy type integral

$$F(z) = \frac{1}{2\pi i} \int_L \frac{f(\zeta)}{\zeta - z} \, d\zeta \tag{2.1}$$

where ζ is a point of the contour L and f is a complex function, defined on L and continuous on each of the separate contours L_ℓ. It is readily observed that the Cauchy type integral describes a sectionally analytic function F, which consists of analytic functions F^- and F^+_ℓ in the regions D^- and D^+_ℓ, $\ell = 1, 2, \ldots, n$. (The proof of analyticity consists in establishing the differentiability with respect to the parameter z.) The density function f determines the jump of the function F across L, that is the difference of the limiting values of functions F^+_ℓ and F^- as z approaches the point ζ_0 on the contour L_ℓ:

$$F^+_\ell(\zeta_0) - F^-(\zeta_0) = f(\zeta_0) \tag{2.2}$$

The proof of Equation (2.2) for a continuous density function f is given by Muskhelishvili, Reference 5, § 18. Assuming that none of the contours L_ℓ passes through the point at infinity, the Cauchy type integral vanishes at infinity:

$$F^-(\infty) = 0 \tag{2.3}$$

The Cauchy type integrals are known to be closely related to the (logarithmic) potentials of simple and double layers, see Reference 5, § 11. However, for the purpose of modelling the flow fields it appears more convenient to identify the function F with the complex disturbance velocity

$$F(z) = U(z) - iV(z) \tag{2.4}$$

where U and V are the x and y-components of the disturbance velocity. Since in two-dimensional potential flow the velocity field is continuous even in the lifting case, there is no need to introduce discontinuity lines (barriers) in the flow region D^-.

It is natural to ask now whether two different density functions can generate one and the same function F^- in the exterior region D^-. As shown below, the answer is affirmative.

Denoting these density functions f_1 and f_2, Equation (2.1) gives the corresponding condition

$$\frac{1}{2\pi i} \int_L \frac{f_1(\zeta) - f_2(\zeta)}{\zeta - z} \, d\zeta = 0, \quad z \in D^-$$

By the interior Cauchy integral formula, Reference 5, § 24, the difference

$$\varphi(\zeta) = f_1(\zeta) - f_2(\zeta)$$

is then the boundary value of the function

$$\varphi(z) = \frac{1}{2\pi i} \int_L \frac{\varphi(\zeta)}{\zeta - z} \, d\zeta, \qquad z \in D^+$$

which is analytic in D^+ and continuous in $D^+ \cup L$. In practical terms this means that on L_ϱ the density $f(\zeta)$ of the Cauchy type integral is determined by the function F^- to within the boundary value $\varphi_\varrho(\zeta)$ of any function $\varphi_\varrho(z)$ analytic in the interior region D_ϱ^+.

Considering the above degree of arbitrariness, one can impose on the density function various constraints, which are convenient from the point of view of the boundary value problem in question, see Reference 5, § 67 and § 68, or Reference 6, § 34. For the solutions to potential flow problems as the most appropriate constraint appears the requirement that the density function $f(\zeta)$ be the boundary value of a function $f(z)$, analytic in D^- and continuous in $D^- \cup L$. Under such circumstances the Cauchy type integral, Equation (2.1), reduces to the Cauchy integral, whose value is, see for example Reference 6, § 1

$$\frac{1}{2\pi i} \int_L \frac{f(\zeta)}{\zeta - z}\, d\zeta = \begin{cases} f(\infty), & z \epsilon D^+ \\ -f(z) + f(\infty), & z \epsilon D^- \end{cases} \tag{2.5}$$

In order to examine the physical aspects of solutions based on Equation (2.5), we first rearrange the Cauchy type integral. Introducing the angle ν between the exterior normal to L and the real axis, see Figure 1, we have

$$d\zeta = i e^{i\nu(\zeta)}\, |d\zeta| \tag{2.6}$$

where $|d\zeta|$ is the contour length element. The density function can be expressed as

$$f(\zeta) = -[\sigma(\zeta) + i\gamma(\zeta)]\, e^{-i\nu(\zeta)} \tag{2.7}$$

where the real functions σ and γ are called the source and vortex densities respectively. The terminology becomes clear when Equations (2.6) and (2.7) are substituted in Equation (2.1). The resultant integral

$$F(z) = \int_L \left[\frac{\sigma(\zeta)}{2\pi(z - \zeta)} + \frac{i\gamma(\zeta)}{2\pi(z - \zeta)} \right] |d\zeta| \tag{2.8}$$

contains singular terms

$$\frac{1}{2\pi(z - \zeta)} \quad \text{and} \quad \frac{i}{2\pi(z - \zeta)}$$

which are recognized as the complex disturbance velocities at z due to the unit strength source and the unit strength vortex located at ζ. Accordingly, the integral of Equation (2.8) will be called the distribution of sources and vortices. From the mathematical point of view, Equation (2.8) is equivalent to Equation (2.1), so that the theory of the Cauchy type integral can be applied to the distribution of sources and vortices whenever necessary.

Turning back to Equation (2.4), we can express the component of the disturbance velocity in the direction of the unit vector exp (iλ) as

$$U(z) \cos\lambda + V(z) \sin\lambda = \mathrm{Re}\,[F(z)\, e^{i\lambda}]$$

Taking first $\lambda = \nu$ and second $\lambda = \nu + \pi/2$, we obtain from Equations (2.2) and (2.7)

$$\mathrm{Re}\left\{ [F_\ell^+(\zeta) - F^-(\zeta)]\, e^{i\nu(\zeta)} \right\} = -\sigma(\zeta) \tag{2.9}$$

$$\mathrm{Re}\left\{ [F_\ell^+(\zeta) - F^-(\zeta)]\, e^{i[\nu(\zeta) + \pi/2]} \right\} = \gamma(\zeta) \tag{2.10}$$

Using the above interpretation, Equations (2.9) and (2.10) indicate that the normal and tangent velocity jumps across L at ζ are given by the values $-\sigma(\zeta)$ and $\gamma(\zeta)$ respectively.

Assuming that the free stream velocity vector is of unit magnitude and at angle α to the real axis, the normal and tangent components of the resultant exterior velocity can be expressed as

$$v(\zeta) = \mathrm{Re}\left\{ [e^{-i\alpha} + F^-(\zeta)]\, e^{i\nu(\zeta)} \right\} \tag{2.11}$$

$$\begin{aligned} u(\zeta) &= \mathrm{Re}\left\{ [e^{-i\alpha} + F^-(\zeta)]\, e^{i[\nu(\zeta) + \pi/2]} \right\} \\ &= -\mathrm{Im}\left\{ [e^{-i\alpha} + F^-(\zeta)]\, e^{i\nu(\zeta)} \right\} \end{aligned} \tag{2.12}$$

The sign convention is such that the normal velocity v is positive in the direction of the outward normal (with respect to the airfoil) and the tangent velocity u is positive in the counterclockwise direction on L.

Using Equations (2.9) and (2.10) we can eliminate F^- from Equations (2.11) and (2.12):

$$v(\zeta) = \mathrm{Re}\left\{ [e^{-i\alpha} + F_\ell^+(\zeta)]\, e^{i\nu(\zeta)} \right\} + \sigma(\zeta) \tag{2.13}$$

$$u(\zeta) = -\mathrm{Im}\left\{ [e^{-i\alpha} + F_\ell^+(\zeta)]\, e^{i\nu(\zeta)} \right\} - \gamma(\zeta) \tag{2.14}$$

In particular, if

$$e^{-i\alpha} + F_\ell^+(\zeta) = 0 \tag{2.15}$$

we obtain

$$v(\zeta) = \sigma(\zeta) \tag{2.16}$$

$$u(\zeta) = -\gamma(\zeta) \tag{2.17}$$

Equations (2.16) and (2.17) will be satisfied along L_ℓ if Equation (2.15) applies everywhere on L_ℓ. By the identity theorem then

$$e^{-i\alpha} + F_\ell^+(z) = 0, \quad z \in D_\ell^+ \tag{2.18}$$

indicating that there is no resultant flow in the interior region L_ℓ.

Conversely, it can be shown that if either Equation (2.16) or Equation (2.17) is valid everywhere on L_ϱ, then the other one is valid too and Equation (2.18) also holds true. Since the establishment of this fact plays a key role in the development of the present vortex panel method, the outline of the proof is presented.

Assuming that Equation (2.16) applies everywhere on L_ϱ, Equation (2.13) gives

$$\mathrm{Re}\left\{\frac{e^{-i\alpha} + F_\varrho^+(\zeta)}{e^{-i\nu(\zeta)}}\right\} = 0, \qquad \zeta \epsilon L_\varrho \tag{2.19}$$

In view of the fact that both the constant $\exp(-i\alpha)$ and the function F_ϱ^+ are analytic in D_ϱ^+, Equation (2.19) specifies a homogeneous Riemann-Hilbert problem for the function ϕ_ϱ^+, analytic in D_ϱ^+ and having the boundary value

$$\phi_\varrho^+(\zeta) = e^{-i\alpha} + F_\varrho^+(\zeta), \qquad \zeta \epsilon L_\varrho$$

Since in going round the contour L_ϱ once in the counterclockwise direction the angle ν acquires the increment 2π, the index of the denominator function, see Reference 6, § 12, is

$$\mathrm{Ind}\,[e^{-i\nu(\zeta)}] = \frac{1}{2\pi} \arg(e^{-i2\pi}) = -1$$

As proved by Gakhov, Reference 6, § 29, for a negative index the interior homogeneous problem does not have a solution. The only possibility to satisfy Equation (2.19) is to require that $\phi_\varrho^+(\zeta) = 0$, $\zeta \epsilon L_\varrho$, i.e. that Equation (2.15) apply all over L_ϱ. The substitution in Equation (2.14) yields Equation (2.17) which completes the proof.

Furthermore, it can be shown that the distribution of sources and vortices, whose density functions are subject to the constraints of Equations (2.16) and (2.17) along the entire contour L, is capable of representing an arbitrary function F^- analytic in the exterior region D^-. To prove this we shall utilize the fact that in this special case the distribution of sources and vortices becomes the Cauchy integral in the true sense. From Equations (2.1) and (2.18) we namely have

$$\frac{1}{2\pi i}\int_L \frac{f(\zeta)}{\zeta - z}\, d\zeta = F_\varrho^+(z) = -e^{-i\alpha}, \qquad z \epsilon D_\varrho^+$$

and consequently, by the exterior Cauchy integral formula, Equation (2.5)

$$\frac{1}{2\pi i}\int_L \frac{f(\zeta)}{\zeta - z}\, d\zeta = -e^{-i\alpha} - f(z), \qquad z \epsilon D^-$$

where $f(z)$ is the analytic continuation of $f(\zeta)$ into the region D^-, taking at the infinitely distant point the value

$$f(\infty) = -e^{-i\alpha}$$

Since the exterior Cauchy formula applies to an arbitrary function f analytic in D^- and continuous in $D^- \cup L$, then also

$$F^-(z) = -e^{-i\alpha} - f(z)$$

is an arbitrary function analytic in D^-. The density function $f(\zeta)$ is uniquely determined from the limiting value of F^- using the relationship

$$f(\zeta) = -e^{-i\alpha} - F^-(\zeta)$$

Having completed this proof, it may be stated that there is no potential flow (past airfoils in free air) whose complex disturbance velocity could not be represented by the distribution of sources and vortices, satisfying Equations (2.16) and (2.17).

Besides expressing the jumps in normal and tangent velocities according to Equations (2.9) and (2.10), the source and vortex densities also acquire a distinct physical meaning when integrated along L, namely that of the discharge and of the circulation.

Since the functions F_ℓ^+ are analytic in the simple connected interior regions D_ℓ^+, they are subject to the Cauchy integral theorem

$$\int_{L_\ell} F_\ell^+(\zeta)\, d\zeta = 0, \qquad \ell = 1, \ldots, n$$

Thus, by the integration of the jump condition, Equation (2.2), and with the help of Equations (2.6) and (2.7) we have

$$\int_L F^-(\zeta)\, d\zeta = -\int_L f(\zeta)\, d\zeta$$

$$= -\int_L \gamma(\zeta)|d\zeta| + i\int_L \sigma(\zeta)|d\zeta| \tag{2.20}$$

From Equations (2.11), (2.12), and (2.6) also

$$\int_L F^-(\zeta)\, d\zeta = \int_L u(\zeta)|d\zeta| + i\int_L v(\zeta)|d\zeta|$$

$$= -\Gamma + iQ \tag{2.21}$$

where

$$Q = \int_L v(\zeta)|d\zeta| = \int_L \sigma(\zeta)|d\zeta| \tag{2.22}$$

is the discharge (efflux) through L and

$$\Gamma = -\int_L u(\zeta)|d\zeta| = \int_L \gamma(\zeta)|d\zeta| \tag{2.23}$$

is the circulation around L. Of course, in the case that Equations (2.16) and (2.17) apply, Equations (2.22) and (2.23) are immediately apparent.

The discharge and the circulation play an important role in the far field approximation of the complex disturbance velocity. Assuming that the airfoil is located near the point z_o, we can expand F^- for large $|z - z_o|$ in the Laurent series

$$F^-(z) = \sum_{m=1}^{\infty} c_m (z - z_o)^{-m}$$

where

$$c_m = \frac{1}{2\pi i} \int_L (\zeta - z_o)^{m-1} F^-(\zeta)\, d\zeta$$

The constant term c_o is missing because of Equation (2.3). Using Equation (2.21) we have

$$F^-(z) = Q \frac{1}{2\pi(z - z_o)} + \Gamma \frac{i}{2\pi(z - z_o)} + O\left(\frac{1}{z - z_o}\right)^2, \quad (z - z_o) \to \infty \tag{2.24}$$

Hence, far from the airfoil the complex disturbance velocity can be approximated by a point source of strength Q and by a point vortex of strength Γ, located at z_o.

3.0 AIRFOIL BOUNDARY VALUE PROBLEM

Assuming the free stream velocity to be of unit magnitude and at angle α to the real axis, the airfoil boundary condition can be written, in accordance with Equation (2.11)

$$\mathrm{Re}\left\{ [e^{-i\alpha} + F^-(\zeta)]\, e^{i\nu(\zeta)} \right\} = v(\zeta) \tag{3.1}$$

The normal component v of velocity is regarded as a given function of L. If the flow is tangent to the contour, then $v(\zeta) \equiv 0$. The use of nonzero values of v serves the purpose of approximating the displacement effect of thin boundary layers in terms of flow through the airfoil contour. Based on the concept of the displacement flux by Preston, Reference 7, the normal component of velocity is set equal to the streamwise derivative of the product of the local potential flow velocity and the displacement thickness of the boundary layer; for more details see Reference 8. Compared to the classical approach by Prandtl, where the displacement thickness is added to the airfoil thickness to produce a modified shape, the Preston concept has the advantage of preserving airfoil geometry in the course of potential flow-boundary layer iterations.

The condition of finite trailing edge velocity — the Kutta-Joukowki condition — can be derived in terms of the source and vortex densities using the properties of the Cauchy type integral, Equation (2.1). From the jump condition of Equation (2.2) it is apparent that for the establishment of the finite velocity field the density f has to be finite everywhere on L. Since a discontinuity in f gives rise to a logarithmic singularity of the Cauchy type integral, see Reference 6, § 8, we require that the density f be continuous on each of the airfoil contours L_ϱ, including the trailing edge point. Denoting by subscripts U and L the upper and lower trailing edge values, we thus require that

$$f_U = f_L \tag{3.2}$$

Applying Equation (2.7), we have

$$(\sigma_U + i\gamma_U)\, e^{-i\nu_U} = (\sigma_L + i\gamma_L)\, e^{-i\nu_L}$$

or

$$\sigma_L + i\gamma_L = -(\sigma_U + i\gamma_U)\, e^{i\theta} \tag{3.3}$$

where

$$\theta = \nu_L - \nu_U - \pi \tag{3.4}$$

is the trailing edge angle, see Figure 2. Thus, Equation (3.3) may be regarded as the Kutta-Joukowski condition expressed in terms of the source and vortex densities.

Independent conditions for the source and vortex densities are obtained from Equation (3.3) in the following special cases:

1. blunt trailing edge, $\theta = \pi$

$$\sigma_L = \sigma_U \tag{3.5}$$

$$\gamma_L = \gamma_U \tag{3.6}$$

2. cusped trailing edge, $\theta = 0$

$$\sigma_L = -\sigma_U \tag{3.7}$$

$$\gamma_L = -\gamma_U \tag{3.8}$$

However, if $0 < \theta < \pi$, Equation (3.3) gives

$$\gamma_U = \frac{\sigma_L + \sigma_U \cos\theta}{\sin\theta} \tag{3.9}$$

$$\gamma_L = -\frac{\sigma_U + \sigma_L \cos\theta}{\sin\theta} \tag{3.10}$$

indicating that the trailing edge values of the source and vortex densities are interdependent.

Geometrically, Equations (3.9) and (3.10) express the condition of equal velocities at the upper and lower trailing edge points. This can easily be established by considering the velocity triangles in Figure 2. We have

$$\frac{-u_U}{\cos\theta_U} = \frac{v_U}{\sin\theta_U} = \frac{v_L}{\sin\theta_L} = \frac{u_L}{\cos\theta_L}$$

where

$$\theta = \theta_U + \theta_L$$

Eliminating θ_U and θ_L and expressing u_U and u_L in terms of v_U, v_L, and θ we arrive at the equations

$$u_U = -\frac{v_L + v_U \cos\theta}{\sin\theta} \tag{3.11}$$

$$u_L = \frac{v_U + v_L \cos\theta}{\sin\theta} \tag{3.12}$$

Substituting for the normal and tangent velocities from Equations (2.13) and (2.14) and using Equation (3.4), we again obtain Equations (3.9) and (3.10). In the case that Equations (2.16) and (2.17) apply, the operation is particularly simple; this way of deriving the trailing edge conditions was first used by Dvorak and Woodward, Reference 9. Hence, with respect to the trailing edge velocity the concepts of finiteness and single-valuedness are found to be equivalent.

Going back to Equations (3.11) and (3.12), another important observation can be made. If the normal components of velocity are zero, then also the tangent components vanish and the trailing edge is inevitably a stagnation point. The only exception to this rule is a cusped trailing edge, where Equations (3.11) and (3.12) do not apply. For a cusped trailing edge, $\theta = 0$, we obtain from Equations (3.7) and (3.8) the velocity relationships

$$v_L = -v_U$$

$$u_L = -u_U$$

which do not imply the existence of a stagnation point if $v_L = v_U = 0$. The best known example is the Joukowski airfoil. For a blunt trailing edge, $\theta = \pi$, we obtain from Equations (3.5) and (3.6) the relationships

$$v_L = v_U$$

$$u_L = u_U = 0 \text{ (by definition)}$$

so that again a stagnation point is obtained if $v_L = v_U = 0$.

In conclusion of this section a few general comments will be made concerning the methods of solution of the airfoil boundary value problem specified by Equations (3.1) and (2.3). By substituting in Equation (3.1) from Equation (2.8) we obtain a singular integral equation which contains two unknown real functions σ and γ. From the discussion in Section 2.0 it became already apparent that the most natural approach is to eliminate the source density σ by setting it equal to the prescribed normal component of velocity, Equation (2.16). It was shown that this type of constraint is allowable, since the integral of Equation (2.8) is still capable of representing an arbitrary function F^- analytic in the flow region D^-. In view of the fact that the vortex density γ is the function to be evaluated, we speak of the vortex distribution method. Its important feature is that the Kutta-Joukowski condition for a finite-angle trailing edge is satisfied by simply fixing the trailing edge values of γ from the known values of σ according to Equations (3.9) and (3.10). As shown in Section 2.0, the evaluated distribution of γ gives directly the distribution of the tangent component of velocity, Equation (2.17).

In contrast to the above approach, the source distribution method utilizes the vortex density as a prescribed function, and the source density is the quantity to be solved for. Apart from the requirements of continuity on smoth portions of the contour and of a sufficient degree of freedom to

satisfy the trailing edge condition, the vortex density can be prescribed arbitrarily*. Since neither of the trailing edge values of σ and γ are known a priori, the Kutta-Joukowski condition for a finite-angle trailing edge is more difficult to satisfy. The most frequently used technique, also known as the Douglas-Neumann method, References 1 and 10, satisfies the trailing edge condition in terms of the linear superposition of the "basic flows": the nonlifting flows due to uniform streams at 0 and 90 degree incidences, the circulatory flows due to a prescribed distribution of γ on each airfoil component, and the displacement flow due to the prescribed normal component of velocity along the airfoil contour. Using this approach, Equations (2.16) and 2.17) are not satisfied and therefore the tangent component of velocity has to be obtained by evaluating the integral of Equation (2.8). A complex plane version of this method, using flat panels with constant source and vortex densities, is described in Reference 1 and no attempt has been made to duplicate this effort here. The vortex distribution method is not only more elegant and straightforward but, as the comparisons of computer results in Section 7.0 reveal, also more accurate.

4.0 VORTEX PANEL METHOD

Each of the n airfoil components is approximated by an inscribed polygon as shown on the ℓ-th component in Figure 3. The corner points are numbered counterclockwise, starting with the (upper) trailing edge point, $j = m(\ell - 1) + 1$, and ending again with the (lower) trailing edge point, $j = m(\ell)$. Since on the first airfoil component the number of the upper trailing edge is 1, we define $m(0) = 0$. The last point is the lower trailing edge point of the n-th component; $m(n)$ is therefore the total number of corner points. The density functions σ and γ are assumed to vary linearly over each panel (line segment), be continuous across the corner points on the smooth portions of the airfoil contour, $j = m(\ell - 1) + 2, m(\ell - 1) + 3, \ldots, m(\ell) - 1$, and obey the trailing edge conditions, Equations (3.9) and (3.10), for points $j = m(\ell - 1) + 1$ and $m(\ell)$. The trailing edge angle θ_ℓ is supposed to satisfy $0 < \theta_\ell < \pi$.

Assuming that all corner values σ_j are known from the prescribed distribution of the normal velocity, this leaves $m(\ell) - m(\ell - 1) - 2$ unknown values γ_j of the vortex density on the ℓ-th airfoil component and $m(n) - 2n$ unknown values γ_j for the whole airfoil. They can be found by satisfying the boundary condition, Equation (3.1), at panel midpoints. Since there are $m(n) - n$ panels, the resultant system of linear algebraic equations is overdetermined by n equations. By solving the overdetermined system, we have the boundary conditions satisfied for all panels, but with some error which is subject to minimization. This idea, suggested to the author by his colleague D.J. Jones, appears to have distinct advantages over sacrificing n selected panels by dropping their boundary conditions and concentrating the error there.

Using Equation (2.1) we can express the complex disturbance velocity at the flowfield point z as

$$F^-(z) = \sum_{\ell=1}^{n} \sum_{j=m(\ell-1)+1}^{m(\ell)-1} \Delta_j F^-(z) \qquad (4.1)$$

---

* The Kutta-Joukowski condition indirectly implies that the distribution of the vortex density has to provide the proper amount of circulation around each airfoil component. Apart from this, there are no additional conditions to consider when prescribing the vortex density. As in Reference 6, § 34, the proof can be provided from the conditions of the solubility of the corresponding Riemann-Hilbert problems in the interior regions D_ℓ^+.

where

$$\Delta_j F^-(z) = \frac{1}{2\pi i} \int_{\zeta_j}^{\zeta_{j+1}} \frac{f(\zeta)}{\zeta - z} \, d\zeta \tag{4.2}$$

is the contribution of the j-th panel. Taking into account the linear dependence

$$f(\zeta) = f_j + \frac{f_{j+1} - f_j}{\zeta_{j+1} - \zeta_j} (\zeta - \zeta_j)$$

$$= \frac{f_{j+1} - f_j}{\zeta_{j+1} - \zeta_j} (\zeta - z) + f_{j+1} \frac{z - \zeta_j}{\zeta_{j+1} - \zeta_j} - f_j \frac{z - \zeta_{j+1}}{\zeta_{j+1} - \zeta_j}$$

we obtain

$$\frac{1}{2\pi i} \int_{\zeta_j}^{\zeta_{j+1}} \frac{f(\zeta)}{\zeta - z} \, d\zeta = \frac{f_{j+1} - f_j}{2\pi i} + \frac{1}{2\pi i} \left[f_{j+1} \frac{z - \zeta_j}{\zeta_{j+1} - \zeta_j} - f_j \frac{z - \zeta_{j+1}}{\zeta_{j+1} - \zeta_j} \right] \log \frac{\zeta_{j+1} - z}{\zeta_j - z} \tag{4.3}$$

From Equation (2.7) we have for the j-th panel

$$f_j = -(\sigma_j + i\gamma_j) e^{-i\nu_j} \tag{4.4}$$

$$f_{j+1} = -(\sigma_{j+1} + i\gamma_{j+1}) e^{-i\nu_j} \tag{4.5}$$

where, according to Equation (2.6)

$$e^{i\nu_j} = -i \frac{\zeta_{j+1} - \zeta_j}{|\zeta_{j+1} - \zeta_j|} \tag{4.6}$$

Since $\Delta_j F^-$ is supposed to be discontinuous as z crosses the segment ζ_j, ζ_{j+1} and vanish at $z = \infty$, we select the negative semiaxis as the branch line of the logarithmic function and require that*

$$\log (1 + 0i) = 0$$

As a result

$$\log \frac{\zeta_{j+1} - z}{\zeta_j - z} = \log \left| \frac{\zeta_{j+1} - z}{\zeta_j - z} \right| + i\tau$$

---

* As a rule, computer subprograms for the complex logarithmic function are written to evaluate the "principal value", satisfying these requirements.

where $-\pi \leqslant \tau < \pi$ is the angle obtained by the rotation of the vector $\zeta_j - z$ into the direction of the vector $\zeta_{j+1} - z$, see Figure 3. In the limit as the point z approaches any point of the j-th panel from the flowfield side, τ tends to the value $-\pi$. Thus the complex disturbance velocity induced by the panel at its own midpoint is

$$\Delta_j F^- \left(\frac{\zeta_j + \zeta_{j+1}}{2} \right) = \frac{f_{j+1} - f_j}{2\pi i} - \frac{1}{4}(f_{j+1} + f_j) \tag{4.7}$$

Denoting the midpoint of the k-th panel

$$z_k = \frac{1}{2}(\zeta_k + \zeta_{k+1}) \tag{4.8}$$

and using Equations (4.1) to (4.7), we obtain

$$F^-(z_k) = \sum_{j=1}^{m(n)} C_{k,j} (\sigma_j + i\gamma_j) \tag{4.9}$$

where

$$C_{k,j} = K_{k,j} + L_{k,j} \tag{4.10}$$

$$K_{k,j} = \begin{cases} \dfrac{1}{2\pi i} e^{-i\nu_j} \left[1 + \dfrac{z_k - \zeta_{j+1}}{\zeta_{j+1} - \zeta_j} \log \dfrac{\zeta_{j+1} - z_k}{\zeta_j - z_k} \right], & j \neq k, m(\ell) \\ \left(\dfrac{1}{4} + \dfrac{1}{2\pi i} \right) e^{-i\nu_k}, & j = k \\ 0, & j = m(\ell) \end{cases} \tag{4.11}$$

$$L_{k,j} = \begin{cases} -\dfrac{1}{2\pi i} e^{i\nu_{j-1}} \left[1 + \dfrac{z_k - \zeta_{j-1}}{\zeta_j - \zeta_{j-1}} \log \dfrac{\zeta_j - z_k}{\zeta_{j-1} - z_k} \right], & j \neq m(\ell - 1) + 1, k + 1 \\ \left(\dfrac{1}{4} - \dfrac{1}{2\pi i} \right) e^{-i\nu_k}, & j = k + 1 \\ 0, & j = m(\ell - 1) + 1 \end{cases} \tag{4.12}$$

Using Equation (2.16) and applying the airfoil boundary condition, Equation (3.1), at panel midpoints z_k, we obtain

$$\mathrm{Re} \left\{ [e^{-i\alpha} + F^-(z_k)] e^{i\nu_k} \right\} = \frac{1}{2}(\sigma_k + \sigma_{k+1}) \tag{4.13}$$

or, with the help of Equation (4.9)

$$\sum_{j=1}^{m(n)} \mathrm{Im}\,(e^{i\nu_k} C_{k,j})\gamma_j = \mathrm{Re}\left[e^{i\nu_k}(e^{-i\alpha} + \sum_{j=1}^{m(n)} C_{k,j}\,\sigma_j)\right] - \frac{1}{2}(\sigma_k + \sigma_{k+1}), \qquad k \neq m(\ell)$$

Introducing the index $K = k + \ell$, this equation can be written in the matrix form

$$A_{K,j}\gamma_j = b_K, \qquad \begin{matrix} K = 1, 2, \ldots, m(n) + n \\ j = 1, 2, \ldots, m(n) \end{matrix} \tag{4.14}$$

where

$$A_{k+\ell,j} = \mathrm{Im}\,(e^{i\nu_k} C_{k,j}), \qquad k \neq m(\ell - 1), m(\ell) \tag{4.15}$$

$$b_{k+\ell} = \mathrm{Re}\left[e^{i\nu_k}(e^{-i\alpha} + \sum_{j=1}^{m(n)} C_{k,j}\sigma_j)\right] - \frac{1}{2}(\sigma_k + \sigma_{k+1}), \quad k \neq m(\ell - 1), m(\ell) \tag{4.16}$$

The elements of rows $m(\ell-1) + \ell$ and $m(\ell) + \ell$ are obtained from the trailing edge conditions, Equations (3.9) and (3.10):

$$A_{m(\ell-1)+\ell,j} = \begin{cases} 1, & j = m(\ell-1) + 1 \\ 0, & \text{otherwise} \end{cases} \tag{4.17}$$

$$b_{m(\ell-1)+\ell} = \frac{\sigma_{m(\ell)} + \sigma_{m(\ell-1)+1}\cos\theta_\ell}{\sin\theta_\ell} \tag{4.18}$$

$$A_{m(\ell)+\ell,j} = \begin{cases} 1, & j = m(\ell) \\ 0, & \text{otherwise} \end{cases} \tag{4.19}$$

$$b_{m(\ell)+\ell,j} = -\frac{\sigma_{m(\ell-1)+1} + \sigma_{m(\ell)}\cos\theta_\ell}{\sin\theta_\ell} \tag{4.20}$$

Utilizing the rotation of unit trailing edge vectors, the cosine and the sine of the trailing edge angle θ_ℓ are obtained as the real and imaginary parts of the expression

$$\cos\theta_\ell + i\sin\theta_\ell = \frac{\zeta_{m(\ell)-1} - \zeta_{m(\ell)}}{|\zeta_{m(\ell)-1} - \zeta_{m(\ell)}|} \; \frac{|\zeta_{m(\ell-1)+2} - \zeta_{m(\ell-1)+1}|}{\zeta_{m(\ell-1)+2} - \zeta_{m(\ell-1)+1}} \tag{4.21}$$

To obtain a least squares solution to the overdetermined system described by Equation (4.14), we first premultiply both sides by the transpose matrix $A_{j,K}$:

$$(A_{j,K}\ A_{K,j})\gamma_j = A_{j,K}\ b_K \tag{4.22}$$

Assuming that the panels do not overlap or cross, that is have no common points other than the corners, the $[m(n) + n] \times m(n)$ matrix $A_{K,j}$ is of rank $m(n)$. Then the square $m(n) \times m(n)$ matrix $(A_{j,K}\ A_{K,j})$ is nonsingular and of rank $m(n)$. Consequently, the system of Equation (4.22) possesses a unique solution which may be found by the LU factorization or other efficient methods for solving systems of linear algebraic equations. Using the fact that the matrix $(A_{j,K}\ A_{K,j})$ is symmetric positive-definite, one can use with great advantage Crout's factorization scheme, Reference 11, § 2.3.4.1, selecting the pivots in order along the diagonal, as suggested in Reference 12.

Denoting by

$$r_K = b_K - A_{K,j}\ \gamma_j$$

the residual of the original system, it can be shown see for example Reference 13, § 5.6, that the solution of Equation (4.22) minimizes the sum

$$\sum_{K=1}^{m(n)+n} r_K^2$$

Of course, there are other methods for solving the overdetermined system of Equation (4.14), such as the minimization of the L_1 norm of the residuals,

$$\sum_{K=1}^{m(n)+n} |r_K|$$

or the minimization of the maximum residual (L_∞ or Chebyshev norm)

$$\max_K |r_K|$$

These solutions can also be very efficient when based on linear programming techniques, see References 14 to 17. As demonstrated on examples in Section 7.0, from the aerodynamic point of view they give almost identical results as the least squares solution. However, they can be of great value especially if the system (4.14) is ill-conditioned due to the occurence of nearly coinciding panels, since the condition of Equation (4.22), on which the least squares solution is based, is worse than that of Equation (4.14), see Reference 13, § 8.8. Otherwise, the least squares solution offers better economy when repeated computations for the same airfoil configuration are required, such as in iterative coupling of the potential flow and boundary layer computations. The advantage of the least squares solution is that it is possible to generate the inverse of the matrix $A_{j,K}\ A_{K,j}$ so that the subsequent computations are reduced to the matrix multiplication of the inverse by the new right hand side $A_{j,K}\ b_K$.

Once the values γ_j of the vortex density have been obtained, the corner values of tangent velocity are known from Equation (2.17). Using the Bernoulli theorem, the pressure coefficients are

evaluated as

$$C_p(\zeta_j) = 1 - (\sigma_j^2 + \gamma_j^2) \tag{4.23}$$

Admittedly, Equations (4.1) to (4.6) indicate at the same time that the complex disturbance velocity is singular at the corner points ζ_j of the polygon, with the exception of the trailing edge where the Kutta-Joukowski condition is satisfied. However, the trailing edge is real whereas other corners lie on smooth portions of the original airfoil contour. If we accept the panel method just as a numerical technique which allows us to discretize the continuous mathematical model in order to evaluate the flow quantities at the points of a smooth contour — and not at corner points of an approximation polygon — the evaluation of the pressure coefficient from Equation (4.23) is justifiable. Comparisons with exact flow solutions fully confirm this philosophy. The advantage of the present approach is that the pressure coefficients are evaluated directly at the contour input points whereas most panel methods give output at panel midpoints, which in fact are not points of the contour.

5.0 DISTRIBUTION OF SOURCES AND VORTICES MODIFIED TO INCLUDE THE WALL INTERFERENCE EFFECT

It is assumed that the flow region is bounded from the outside by two parallel, infinite wind tunnel walls at $y = h/2$ and $-h/2$, see Figure 4, and that the walls behave in such a way that the normal component of velocity is proportional to the pressure drop across the wall (Darcy law). We have mainly the perforated walls in mind, but indications are that even slotted walls behave to some extent like this, Reference 18.

If the pressure outside the walls (the plenum pressure) is equal to the static pressure of the wind tunnel stream infinitely far upstream, then the normal component of velocity is proportional directly to the wall pressure coefficient. In the wind tunnel, the flow infinitely far upstream is supposed to be at angle $\alpha = 0$ with respect to the x-axis, so that in terms of complex disturbance velocity the normal component of velocity is $-\text{Im } F^-$ on the upper wall and $\text{Im } F^-$ on the lower wall. Assuming further that the airfoil induces small pressure disturbances at the walls, the pressure coefficient can be linearized and expressed as $-2 \text{ Re } F^-$. Summarizing this, we obtain the following boundary conditions for upper and lower walls

$$P_U \text{ Re } F^-(z) - \text{Im } F^-(z) = 0, \qquad z = x + i\,h/2 \tag{5.1}$$

$$P_L \text{ Re } F^-(z) + \text{Im } F^-(z) = 0, \qquad z = x - i\,h/2 \tag{5.2}$$

The positive constants P_U and P_L, called the porosity parameters or resistance factors for upper and lower walls, have to be determined experimentally for given walls and specific flow conditions; either directly, Reference 18, or indirectly, Reference 4. The solutions based on Equations (5.1) and (5.2) contain, as limiting cases, those for a solid wall wind tunnel ($P_U = P_L = 0$) and for an open jet wind tunnel ($P_U, P_L \to \infty$). The reason for using different porosity parameters for upper and lower walls is that the walls may actually be of different open area ratios or, even if identical, they may display a different resistance to outflow than to inflow, see for example Reference 4. Under the latter circumstance, Equations (5.1) and (5.2) are not suited for mixed inflow-outflow conditions, but apply well if along each wall either the inflow or outflow conditions prevail, as is the case of high lift systems (inflow on the suction side and outflow on the pressure side of the airfoil).

Since Equations (5.1) and (5.2) are linear and homogeneous with respect to the real and imaginary parts of F^-, we may use the concept of a Green's function to express the complex disturbance velocity of the wind tunnel flow past a multi-component airfoil as a line integral along the airfoil

contour. In the context of Green's theorems and eigenfunction expansions, the basic idea of this approach was first given by Kacprzynski, Reference 19.

Assuming that the airfoil is positioned inside the wind tunnel,

$$|\mathrm{Im}\zeta| < h/2, \qquad \zeta \in L$$

we can write, in analogy to Equation (2.8)

$$F(z) = \int_L [\sigma(\zeta)G_\sigma(z,\zeta) + \gamma(\zeta)G_\gamma(z,\zeta)]\,|d\zeta| \tag{5.3}$$

where

$$G_\sigma(z,\zeta) = \frac{1}{2\pi(z-\zeta)} + H_\sigma(z,\zeta) \tag{5.4}$$

$$G_\gamma(z,\zeta) = \frac{i}{2\pi(z-\zeta)} + H_\gamma(z,\zeta) \tag{5.5}$$

are the Green's functions (influence functions).

The first right hand terms, generally called the fundamental solutions, are singular at $z = \zeta$ and vanish at $z = \infty$. They are recognized as complex disturbance velocities at z due to a point source and a point vortex at ζ, as if no walls were present. The functions H_σ and H_γ are analytic in the strip $|\mathrm{Im}z| < h/2$ and such that both G_σ and G_γ satisfy the wall boundary conditions of Equations (5.1) and (5.2). In terms of a two-argument Green's function G (= G_σ or G_γ) these conditions read

$$P_U \ \mathrm{Re}\, G(z,\zeta) - \mathrm{Im}\, G(z,\zeta) = 0, \qquad z = x + i\,h/2 \tag{5.6}$$

$$I'_L \ \mathrm{Re}\, G(z,\zeta) + \mathrm{Im}\, G(z,\zeta) = 0, \qquad z = x - i\,h/2 \tag{5.7}$$

for any $|\mathrm{Im}\zeta| < h/2$. Consequently, the functions H_σ and H_γ can be interpreted as complex disturbance velocities at z induced by the wind tunnel walls as a response to the presence of a point source and a point vortex at ζ, respectively. Using Equations (5.4) to (5.7) it can be shown that the integral of Equation (5.3) satisfies the wall boundary conditions, Equations (5.1) and (5.2), for arbitrary density functions σ and γ.

Solving the boundary value problem of Equations (5.6) and (5.7) for the Green's functions defined by Equations (5.4) and (5.5) by the image method of Ebihara, Reference 20, the analytic parts are found to be, Reference 3:

$$H_\sigma(z,\zeta) = B(z,\zeta) + E(z,\zeta) + C \tag{5.8}$$

$$H_\gamma(z,\zeta) = i\,[B(z,\zeta) - E(z,\zeta)] \tag{5.9}$$

where

$$B(z,\zeta) = \frac{1}{2h} \frac{e^{\pi \frac{t_U + t_L}{2} \frac{z-\zeta}{h}}}{e^{\pi \frac{z-\zeta}{h}} - 1} - \frac{1}{2\pi(z-\zeta)} \tag{5.10}$$

$$E(z,\zeta) = -\frac{1}{2h} \frac{e^{\pi \frac{t_U + t_L}{2} \frac{z-\bar{\zeta}}{h}}}{e^{\pi \frac{z-\bar{\zeta}}{h}} + 1} e^{i\pi \frac{t_U - t_L}{2}} \tag{5.11}$$

$$C = \begin{cases} \frac{1}{h}, & P_U = P_L = 0 \\ 0, & \text{otherwise} \end{cases} \tag{5.12}$$

In Equation (5.11), $\bar{\zeta}$ denotes the complex conjugate of ζ. The porosity parameters P_U and P_L enter the above formulas through the functions

$$t_U = \frac{2}{\pi} \text{ atan } P_U \tag{5.13}$$

$$t_L = \frac{2}{\pi} \text{ atan } P_L \tag{5.14}$$

which vary on the interval $< 0,1)$.

Further details concerning the derivation are not given here, but the results can easily be verified by direct substitution in Equations (5.6) and (5.7). From Equations (5.6) and (5.7) it is also apparent that the constant C can acquire an arbitrary real value if $P_U = P_L = 0$; otherwise it must be zero. The value $C = 1/h$ selected for the solid wall wind tunnel, $P_U = P_L = 0$, satisfies the additional condition

$$\lim_{\text{Re } z \to -\infty} G_\sigma(z,\zeta) = 0$$

by which the undisturbed flow conditions are established infinitely far upstream (but not necessarily far downstream). If at least one of the porosity factors is non-zero, then

$$\lim_{\text{Re } z \to \pm\infty} B(z,\zeta) = \lim_{\text{Re } z \to \pm\infty} E(z,\zeta) = 0$$

so that undisturbed flow conditions are automatically established both upstream and downstream. This basic difference between the solid wall and the porous wall wind tunnels is due to the simplifying

assumption that the walls are of infinite streamwise extent, see Reference 21. In the porous wall wind tunnel the flux due to a source can escape through the walls, no matter how little porous they are, and the undisturbed flow conditions are established infinitely far upstream and downstream. For the solid wall wind tunnel this is not true and the presence of a source is thus felt over the entire wind tunnel length. The only exception is if the discharge Q, Equation (2.22), of the airfoil is zero, so that the wall interference contributions of the source terms cancel out far upstream and downstream. The awareness of the above properties of the wind tunnel flow solutions is very important for the correct interpretation of the results.

It is easily verified that the functions H_σ and H_γ have no singularities other than simple poles outside the wind tunnel. Their locations

$$z = \zeta \pm i\,2kh \qquad , \quad k = 1, 2, 3, \ldots$$

$$z = \bar{\zeta} \pm i(2k - 1)h, \quad k = 1, 2, 3, \ldots$$

are known as "images" of ζ. At $z = \zeta$ the function B has a removable singularity, so that the functions H_σ and H_γ are analytic in the entire wind tunnel interior. In order to calculate their values in the vicinity of point $z = \zeta$, we use the power series expansion, Reference 2:

$$B(z,\zeta) = \frac{1}{2h} \sum_{m=1}^{\infty} B_m \left(\frac{t_U + t_L}{2} \right) \frac{\left(\pi \dfrac{z - \zeta}{h} \right)^{m-1}}{m!}, \qquad \frac{|z - \zeta|}{h} < 2 \tag{5.15}$$

where $B_m(t)$ denotes the Bernoulli polynomial

$$B_m(t) = \sum_{k=0}^{m} \binom{m}{k} B_k\, t^{m-k}, \qquad m = 1, 2, 3, \ldots \tag{5.16}$$

and B_k the Bernoulli number, described by the recursion formulas

$$B_0 = 1$$

$$B_{k+1} = \sum_{j=0}^{k+1} \binom{k+1}{j} B_j, \qquad k = 1, 2, 3, \ldots \tag{5.17}$$

This gives

$$B_1(t) = t - \frac{1}{2}$$

$$B_2(t) = t^2 - t + \frac{1}{6}$$

$$B_3(t) = t^3 - \frac{3}{2} t^2 + \frac{1}{2} t$$

In particular, at $z = \zeta$ we obtain

$$B(z,z) = \frac{1}{2h} B_1 \left(\frac{t_U + t_L}{2} \right)$$

$$= \frac{1}{2h} \left(\frac{t_U + t_L}{2} - \frac{1}{2} \right) \tag{5.18}$$

If the wind tunnel height h becomes infinitely large, the functions H_σ and H_γ vanish, and Equation (5.3) reduces to Equation (2.8), valid for the free air case.

Since the functions H_σ and H_γ are analytic in the entire wind tunnel interior, they must also be continuous across the airfoil contour L and hence cannot affect the jump condition described by Equation (2.2). From this it already follows that Equations (2.9) to (2.19) and conditions under which they were derived remain valid. Consequently, in the vortex distribution method the evaluation of the vortex density γ from the airfoil boundary condition, Equations (3.1) and (2.16), and from Equations (5.3) to (5.5) remains essentially the same as for the free air case. At this stage attention is no longer paid to the wind tunnel boundary conditions, Equations (5.1) and (5.2), since they are automatically satisfied by the properties of the above Green's functions for any distribution of sources and vortices. As in the free air case, the tangent component of velocity is obtained from Equation (2.17) and the pressure coefficient follows from Equation (4.23).

If the airfoil chord to wind tunnel height ratio c/h is small, say 1/4 or less, the wall interference effect in potential flow can be approximated by a single angle of attack correction. Using the analytic part of the integral of Equation (5.3), the angle of attack correction can be expressed as

$$\Delta\alpha = -\mathrm{Im} \int_L [\sigma(\zeta) H_\sigma(z,\zeta) + \gamma(\zeta) H_\gamma(z,\zeta)] \, |d\zeta| \tag{5.19}$$

where z is some reference point inside the airfoil, e.g. the quarter chord point. In order to obtain a formula involving only the integrals of σ and γ, we expand the functions H_σ and H_γ in Taylor expansions about the point z:

$$H(z,\zeta) = H(z,z) + \left. \frac{dH(z,\zeta)}{d\zeta} \right|_{\zeta = z} (\zeta - z) + \ldots$$

Assuming that the angle of attack correction does not vary significantly along the airfoil, we restrict ourselves only to the constant terms. Thus

$$\Delta\alpha = -\mathrm{Im}\left\{ H_\sigma(z,z) \int_L \sigma(\zeta) |d\zeta| + H_\gamma(z,z) \int_L \gamma(\zeta) |d\zeta| \right\}$$

$$= -Q \, \mathrm{Im} \, H_\sigma(z,z) - \Gamma \, \mathrm{Im} \, H_\gamma(z,z)$$

where Q and Γ, Equations (2.22) and (2.23), are the values of the discharge and the circulation, respectively. Of course, the above expression can also be obtained from the far field approximation of F^- in free air, Equation (2.24), employing the source and the vortex strengths, Q and Γ, as the factors of

the analytic parts of Green's functions, Equations (5.4) and (5.5). The values $H_\sigma(z,z)$ and $H_\gamma(z,z)$ can be evaluated from Equations (5.8), (5.9), (5.11), and (5.18). In particular, if the airfoil is located near the tunnel axis, then z = 0 and

$$\Delta\alpha = \frac{Q}{4h}\sin\left(\pi\frac{t_U - t_L}{2}\right) - \frac{\Gamma}{4h}\left[t_U + t_L + \cos\left(\pi\frac{t_U - t_L}{2}\right) - 1\right] \tag{5.20}$$

If the flow is tangent to the airfoil, then Q = 0 and according to the Joukowski theorem approximately

$$\Gamma = \frac{1}{2}\,c\,C_L$$

where C_L is the lift coefficient of the airfoil. As a result

$$\Delta\alpha = -\frac{1}{4}\frac{c}{h}C_L\left\{\frac{t_U + t_L}{2} + \frac{1}{2}\left[\cos\left(\pi\frac{t_U - t_L}{2}\right) - 1\right]\right\} \tag{5.21}$$

which in the case of equal porosity parameters, $P_U = P_L = P$, that is $t_U = t_L = t$, reduces to the familiar formula

$$\Delta\alpha = -\frac{1}{4}\frac{c}{h}C_L t = \frac{c}{h}C_L\delta_0 \tag{5.22}$$

The expression

$$\delta_0 = -\frac{1}{4}t = -\frac{1}{2\pi}\operatorname{atan} P \tag{5.23}$$

is known as the upwash or the lift interference factor.

In order to include terms containing higher powers of the ratio c/h we would have to carry the higher order terms in the Taylor expansions of functions H_σ and H_γ or , if using the far field approximation, the higher terms of the Laurent expansion of F^{-}. It can be shown that in this way the influence of the pitching moment, the cross-sectional area of the airfoil, and the higher moments of the pressure and the thickness distributions can be taken into account. However, if the distributions of σ and γ are known, as in the computations by the present method, one can directly use Equation (5.19).

The corrected lift and drag coefficients C'_L and C'_D are obtained from the wind tunnel values C_L and C_D by resolving the aerodynamic force into the directions parallel and normal to the corrected direction of the wind tunnel stream

$$C'_L = C_L\cos\Delta\alpha - C_D\sin\Delta\alpha \tag{5.24}$$

$$C'_D = C_D\cos\Delta\alpha + C_L\sin\Delta\alpha \tag{5.25}$$

It is perhaps worth mentioning that the drag coefficient C_D, obtained as the nondimensional component of the aerodynamic force parallel to the wind tunnel axis, is as a result of wall interference is in general non-zero even if $Q = 0$.

The angle of attack correction has no direct effect on the pitching moment, that is

$$C'_M = C_M \tag{5.26}$$

The usefulness of the angle of attack correction in practical applications is examined in Section 7.0.

6.0 VORTEX PANEL METHOD FOR THE WALL INTERFERENCE CASE

Using the results of Section 5.0, it is a simple matter to modify the vortex panel algorithm developed in Section 4.0 to include the wall interference effect.

In the presence of wind tunnel walls, Equation (4.2) is replaced by

$$\Delta_j F^-(z) = \frac{1}{2\pi i} \int_{\zeta_j}^{\zeta_{j+1}} \frac{f(\zeta)}{\zeta - z}\, d\zeta + \int_{\zeta_j}^{\zeta_{j+1}} \left[\sigma(\zeta) H_\sigma(z,\zeta) + \gamma(\zeta) H_\gamma(z,\zeta)\right] |d\zeta| \tag{6.1}$$

This follows from Equations (5.3) to (5.5). In order to evaluate the additional integral, we note that the functions H_σ and H_γ, given by Equations (5.8) and (5.9), are analytic in the entire wind tunnel interior in both arguments z and ζ, and can thus be expanded in the following Taylor expansions about the panel midpoint z_j:

$$H(z,\zeta) = H(z,z_j) + \left.\frac{dH(z,\zeta)}{d\zeta}\right|_{\zeta = z_j} (\zeta - z_j) + \ldots$$

Assuming that the length $|\zeta_{j+1} - \zeta_j|$ of the panel is small compared to its distance from the wall $|\pm h/2 - l_m(z_j)|$, we can restrict ourselves only to the constant term in the above expansion. This yields

$$\int_{\zeta_j}^{\zeta_{j+1}} \sigma(\zeta) H_\sigma(z,\zeta) |d\zeta| = \frac{1}{2} (\sigma_j + \sigma_{j+1}) H_\sigma(z,z_j) |\zeta_{j+1} - \zeta_j| \tag{6.2}$$

$$\int_{\zeta_j}^{\zeta_{j+1}} \gamma(\zeta) H_\gamma(z,\zeta) |d\zeta| = \frac{1}{2} (\gamma_j + \gamma_{j+1}) H_\gamma(z,z_j) |\zeta_{j+1} - \zeta_j| \tag{6.3}$$

Introducing complex coefficients

$$S_{k,j} = \begin{cases} \frac{1}{2} H_\sigma(z_k, z_j) |\zeta_{j+1} - \zeta_j| & , \; j = m(\ell-1)+1 \\ \frac{1}{2} H_\sigma(z_k, z_j) |\zeta_{j+1} - \zeta_j| + \frac{1}{2} H_\sigma(z_k, z_{j-1}) |\zeta_j - \zeta_{j-1}| & , \; j \neq m(\ell-1)+1, m(\ell) \\ \frac{1}{2} H_\sigma(z_k, z_{j-1}) |\zeta_j - \zeta_{j-1}| & , \; j = m(\ell) \end{cases} \tag{6.4}$$

$$G_{k,j} = \begin{cases} -\frac{i}{2} H_\gamma(z_k z_j) |\zeta_{j+1} - \zeta_j| & , \; j = m(\ell-1)+1 \\ -\frac{i}{2} H_\gamma(z_k, z_j) |\zeta_{j+1} - \zeta_j| - \frac{i}{2} H_\gamma(z_k, z_{j-1}) |\zeta_j - \zeta_{j-1}| & , \; j \neq m(\ell-1)+1, m(\ell) \\ -\frac{i}{2} H_\gamma(z_k, z_{j-1}) |\zeta_j - \zeta_{j-1}| & , \; j = m(\ell) \end{cases} \tag{6.5}$$

and substituting Equations (6.1) to (6.3) in Equation (4.1), we obtain

$$F^-(z_k) = \sum_{j=1}^{m(n)} (C_{k,j} + S_{k,j}) \sigma_j + i \sum_{j=1}^{m(n)} (C_{k,j} + G_{k,j}) \gamma_j \tag{6.6}$$

which replaces Equation (4.9). As before, the coefficients $C_{k,j}$ are given by Equations (4.10) to (4.12).

Since the oncoming wind tunnel stream is at angle $\alpha = 0$ with the x-axis, the airfoil boundary condition, Equation (4.13), takes the form

$$\mathrm{Re}\left\{ [1 + F^-(z_k)] e^{i\nu_k} \right\} = \frac{1}{2} (\sigma_k + \sigma_{k+1}) \tag{6.7}$$

Substituting for $F^-(z_k)$ from Equation (6.6) we again obtain a set of linear algebraic equations described by Equation (4.14) except that now

$$A_{k+\ell,j} = \mathrm{Im}\left[e^{i\nu_k} (C_{k,j} + G_{k,j}) \right], \quad k \neq m(\ell-1), m(\ell) \tag{6.8}$$

and

$$b_{k+\ell} = \mathrm{Re}\left\{ e^{i\nu_k} \left[1 + \sum_{j=1}^{m(n)} (C_{k,j} + S_{k,j})\, \sigma_j \right] \right\} - \frac{1}{2}(\sigma_k + \sigma_{k+1}), \qquad k \neq m(\ell-1), m(\ell) \qquad (6.9)$$

The elements of the remaining rows follow from the trailing edge conditions and are again given by Equations (4.17) to (4.20).

The overdetermined system of linear algebraic equations is solved as described in Section 4.0 and the values of the airfoil pressure coefficients are obtained from Equation (4.23). The pressure coefficients along the wind tunnel walls can be evaluated from Equations (4.1) and (6.1) to (6.3), using the Bernoulli theorem:

$$C_p(z) = 1 - |1 + F^-(z)|^2 \qquad (6.10)$$

where

$$\mathrm{Im}\,(z) = \pm h/2$$

In comparison with experimental wall pressure coefficients, they can be used to provide a posteriori check on the values P_U and P_L which were used in the above computation. A practical implementation of this technique has been reported in Reference 4.

7.0 NUMERICAL EXAMPLES

In order to demonstrate the accuracy and efficiency of the present vortex panel method, example computations are performed for some theoretical profiles, whose exact potential flow solutions are known. The exact solutions assume tangent flow conditions all over the airfoil, so that stagnation points are obtained at finite-angle trailing edge.

First, a circulatory flow past the unit circle is evaluated. The corner points are selected at

$$\zeta_k = e^{i2\pi(k-1)/36}, k = 1, 2, \ldots, 37$$

and a 10 degree angle of attack is assumed, $\alpha = \pi/18$. Table 1 compares the exact pressure coefficients with the L.S. (least squares), L_1, and L_∞ solutions. It is observed that the agreement with the exact solution is excellent, and that all three methods give practically identical results. From the technical point of view it does not seem to make much difference which type of the residual norm is minimized. As far as the cost is concerned, the execution time for the single precision vortex panel method on the IBM 370/3032 computer was 0.5 sec. for the L.S. solution, 0.7 sec. for the L_1 solution, and 0.6 sec. for the L_∞ solution.

Table 2 presents the results of similar computations on the cambered Kármán-Trefftz airfoil, whose co-ordinates are obtained using the mapping function

$$\frac{\zeta_k - ps}{\zeta_k + ps} = \left(\frac{\hat{\zeta}_k - s}{\hat{\zeta}_k + s} \right)^p, \quad p = 179/90, \; s = 0.92$$

from the unit circle co-ordinates

$$\hat{\zeta}_k = s + \left[e^{i\,2\pi(k-1)/36} - 1\right] e^{-i\epsilon}, \epsilon = \pi/36, k = 1, 2, \ldots, 37$$

By the Schwarz-Christoffel theorem, the theoretical trailing edge angle is $\Theta = \pi(2 - p) = \pi/90$, that is two degrees. The flow is assumed to be at zero incidence with respect to the real axis, $\alpha = 0$. Compared to the circle, the agreement between the exact and computed pressure distributions on the Kármán-Trefftz airfoil is not as good, notably in the vicinity of the sharp trailing edge. Substantial improvement in accuracy can be achieved by doubling the number of panels as demonstrated in Table 3, but of course at the increased cost of computation. The L.S., L_1, and L_∞ solutions took 2.5, 4.0, and 2.9 sec., respectively. However, from Figure 5, showing the exact and the L.S. solutions in the unit chord scale, it may be seen that with 72 panels the agreement is more than satisfactory.

As the third test example is chosen the two-component airfoil by Williams, Reference 22. The contour points of the "Configuration A", tabulated in Reference 22, are directly taken as the corner points for the present vortex panel method. Table 3 compares the pressure coefficients by Williams (CP EXACT) with the computed ones by the present method, using the least squares mode (CP L.S.). From the pressure curves in Figure 6 it is seen that the vortex panel method predicts correctly the suction peaks on both airfoil components and that the overall agreement is excellent except in the trailing edge region of the main airfoil. In conjunction with vortex panel methods, a similar trailing edge discrepancy on the Williams' airfoil was also observed by Choo, Reference 23, but apparently not by Weibust, Reference 24, who did not force the flow through stagnation points at the trailing edges, assuming that they behaved like cusps. However, since the Williams' pressure coefficients were verified to within a three digit accuracy by Ives, Reference 25, using a modernized Theodorsen-Garrick conformal mapping technique for the analysis of two-component airfoils, it is safe to assume that the observed trailing edge discrepancy is the liability of the present vortex panel method. Using this and the preceding example, one may conjecture that it is difficult to correctly reproduce large pressure gradients near trailing edges unless the number of panels is increased significantly. The mapping of the trailing edge onto a circular segment is by its nature much better suited for the task. Nevertheless, the main attractiveness of the panel method is its simplicity and direct applicability to airfoils having a number of components larger than two, where the method of Reference 25 cannot be used, and to complex geometric configurations, such as multi-component airfoils between wind tunnel walls. Apparently, one could exploit the advantages of both techniques by removing sharp trailing edges (or edges having a small radius of curvature) by Kármán-Trefftz transformations and applying the panel method to the transformed configuration. However, since complications arise with regard to the present treatment of the wall interference effect and, in addition to it, the conformal mapping techniques seem to fall somewhat outside the scope of the present report, no example is given here.

To obtain the overall comparison between the computed and the theoretical results, Table 5 presents the lift and drag force coefficients, obtained by the integration of pressure distributions. Compared are the exact values and the computations by the source panel method (Douglas-Neumann type) from Reference 22 with the computations by the present vortex panel method. The integration of pressure coefficients over the co-ordinate points of Table 4 is performed using the method by Nonweiler, Reference 26. The force coefficients are normalized by the chord length $c = 1.33$. It is observed that the present method predicts the lift forces with a better accuracy than the source panel method, but more importantly, the resultant drag force is only 0.0006, which is acceptably close to the zero value according to the d'Alembert paradox. This result indicates that the present method is accurate enough to be used in conjunction with viscous calculations for the evaluation of drag.

The column CPW L.S. in Table 4 gives the pressure coefficients calculated by the present method (in the least squares mode) for the following wall interference case: $c/h = 0.25$, $P_U = 1.2$, $P_L = 0.8$. As before, the airfoil is at zero incidence with respect to the direction of stream at infinity (the wind tunnel axis). Due to the wall effect, the lift force decreases from its free air value of

2.7887 to 2.2854 and the drag force increases from 0.0006 to 0.1598, cf. Tables 5 and 6. In order to clarify the major trends of these changes, Equation (5.21) is used to evaluate the angle of attack correction $\Delta\alpha = -3.958$ deg. and the lift and drag coefficients are corrected according to Equations (5.24) and (5.25). From Table 6 it is seen that the correction value 2.2910 does not greatly differ from the uncorrected value 2.2854, but the effect on the drag coefficient is substantial: the corrected value 0.0016 is again very close to zero. For comparison, in column CPF L.S. on Table 4 printed are pressure coefficients of the free air case at the angle of attack $\alpha = -3.958$ deg. The values of the lift and the drag coefficients, obtained by the integration of pressure coefficients, are given in Table 6. The departure of the free air value 2.3468 of the lift coefficient from the corrected wind tunnel value 2.2910 can be verified on the difference of pressure curves in Figure 7. The corresponding drag loops are displayed in Figure 8. Here the pressure coefficients on the main airfoil and the flap plotted against the co-ordinate

$$y_n = (y - y_t)\cos\alpha - (x - x_t)\sin\alpha$$

where x_t, y_t is the respective trailing edge. It is observed that in free air the negative contribution of the main airfoil is counterbalanced by the positive contribution of the flap. In the wind tunnel case the flap contributes considerably more than the main airfoil, but the balance of drag contributions is regained by applying the angle of attack correction to the co-ordinate y_n. However, the remaining differences between the pressures in the free air case and the corrected wind tunnel case which are observed on upper surfaces of both the main airfoil and the flap are again of the same magnitude as those seen in Figure 7. This indicates that the wind tunnel case corrected for $\Delta\alpha$ and the free air case are not exactly the same*. The difference between the two flow patterns is also apparent on the pressure distributions computed at the location of the walls, Figure 9. Although the airfoil in the wind tunnel at $\alpha = 0$ deg. and in free air at $\alpha = -3.958$ deg. produces nearly the same amount of lift, the wall pressure signatures differ considerably.

A more direct approach is to avoid the concept of the angle of attack correction altogether and interpret the corrections to pressures, force and pitching moment coefficients, and other aerodynamic quantities of interest as the differences between their free air and wind tunnel values, computed at the same angle of attack. For example, as the corrections to pressure coefficients on the Williams' airfoil we can use the differences between the values CP L.S. and CPW L.S. in Table 4. Another example is given in Figure 10 where the lift coefficient C_L, the drag coefficient C_D, and the quarter-chord pitching moment coefficient C_M are evaluated on the Williams' airfoil in free air and the wind tunnel, at angles of attack -6, -4, -2, 0, and 2 deg. Using the interpolation curves, corrections to C_L, C_D, and C_M can be found on the whole interval $-6 \text{ deg.} \leqslant \alpha \leqslant 2$ deg. Naturally, this approach can be of practical value for correcting the wind tunnel data only after the viscous effects on the airfoil have been incorporated and the selected values of porosity parameters checked by comparing the experimental and computed wall pressure distributions.

For comparison, in Figure 10 are as dash-dotted lines also drawn the wind tunnel values of C_L, C_D, and C_M at $\alpha = -4, -2, 0$, and 2 deg., corrected according to Equations (5.24) to (5.26) for a variable (negative) $\Delta\alpha$. It is seen, for example, that the line of corrected C_L at $\alpha = 0$ deg. intersects the line of free air C_L near $\alpha = -4.4$ deg., but the corrected wind tunnel C_D at $\alpha = 0$ deg. agrees with the free air C_D near $\alpha = -4.0$ deg. — a difference of 0.4 deg. Apparently, with respect to the force coefficients the angle of attack correction is a tool suffering from a great deal of astigmatism in this particular case: we can either focus on the free air C_D or on the free air C_L, but not at both at once. As far as the pitching moment is concerned, the situation is even worse: we are completely out of "focus" in the given interval of angles of attack. (In absolute terms, however, the difference between the two sets of C_M values is quite small.)

---

* From the engineering point of view, however, these differences may be considered insignificant.

It should be realized that the studied wall interference example is somewhat arbitrary, although by no means unrealistic. However, it serves to illustrate that the simple angle of attack correction procedure may have certain limitations, especially when applied to high lift systems.

As pointed out above, since the present method can be used to compute both the free air and the wind tunnel cases at the same angle of attack, the difference of these sets of data can directly be used as correction to the measured wind tunnel data. This process would eliminate the need for angle of attack correction. Furthermore, in conjunction with the modelling of displacement effects the present method also contains the mechanism by which the wall effects on the development of boundary layers can be accounted for — something that cannot be done with conventional wall correction techniques.

On the IBM 370/3032 computer the execution time required to compute the 122 panel Williams' airfoil was 9.6 sec. in the free air case and 17.4 sec. in the wind tunnel case. The increase of the computation time in the wind tunnel case is due to the fact that the elements of the matrix carry additional terms which require the computation of Green's function values. In the case that the inverse of the matrix has been generated, the repeated computation for a different angle of attack takes only about 0.2 sec. in the free air case. For the wind tunnel case, unfortunately, any change of angle of attack gives rise to a completely new airfoil-wind tunnel configuration so that a new matrix has to be assembled each time. However, for repeated computations where only the normal component of velocity is affected (iterations on the boundary layer displacement effect), the matrix of the system does not change so that the subsequent use of its inverse brings about the same time economy as in the free air case.

8.0 CONCLUSIONS

The developed vortex panel algorithm for the computation of potential flow past two-dimensional airfoils is very simple and efficient, and at the same time capable of providing sufficient accuracy for most practical applications. For a further improvement in the reproduction of large pressure gradients near sharp trailing edges, or edges having a small radius of curvature, the use of the present method in conjunction with conformal mapping techniques is recommended. However, even in its present form it yields ample accuracy to permit analysis of such effects as the inviscid drag induced by porous wind tunnel walls. It is believed that the present method will help to accomplish the main objective — the prediction of the aerodynamic performance of high lift systems in free air and in the wind tunnel, with the consideration of viscous effects.

9.0 ACKNOWLEDGEMENTS

The author wishes to express his sincere appreciation to Mr. D.J. Jones of the High Speed Aerodynamics Laboratory and to Dr. N.N. Abdelmalek of the Division of Electrical Engineering, National Research Council of Canada, for their valuable suggestions and computer programs for the solution of overdetermined systems of linear algebraic equations.

10.0 REFERENCES

1. Giesing, J.P. *Potential Flow About Two-Dimensional Airfoils.* LB 31946, Douglas Aircraft Co., December 1965.

2. Mokry, M. *Calculation of Flow Past Multi-Component Airfoils in Perforated Wind Tunnel.* C.A.S.I. Transactions, Vol. 7, 1974, pp. 19-24.

3. Mokry, M. — *Integral Equation Method for Subsonic Flow Past Airfoils in Ventilated Wind Tunnels.* AIAA Journal, Vol. 13, 1975, pp. 47-53.

4. Mokry, M., Peake, D.J., Bowker, A.J. — *Wall Interference on Two-Dimensional Supercritical Airfoils, Using Wall Pressure Measurements to Determine the Porosity Factors for Tunnel Floor and Ceiling.* NRC/Aero Report LR-575, National Research Council Canada, Ottawa, Ontario, February 1974.

5. Muskhelishvili, N.I. — *Singular Integral Equations.* Noordhoff, Groningen-Holland, 1953.

6. Gakhov, F.D. — *Boundary Value Problems.* Pergamon Press, 1966.

7. Preston, J.H. — *The Effect of the Boundary Layer and Wake on the Flow Past a Symmetrical Aerofoil at Zero Incidence.* R. & M. No. 2107, A.R.C. Technical Rept., July 1945.

8. Lighthill, M.J. — *On Displacement Thickness.* J. Fluid Mech., Vol. 4, 1958, pp. 383-392.

9. Dvorak, F.A., Woodward, F.A. — *A Viscous/Potential Flow Interaction Analysis Method for Multi-Element Infinite Swept Wings.* NASA CR-2476, November 1974.

10. Hess, J.L., Smith, A.M.O. — *Calculation of Potential Flow About Arbitrary Bodies.* Progress in Aeronautical Sciences, Vol. 8, Pergamon Press, 1966.

11. Westlake, J.R. — *A Handbook of Numerical Matrix Inversion and Solution of Linear Equations.* J. Wiley & Sons, 1968.

12. Martin, R.S., Wilkinson, J.H. — *Symmetric Decomposition of Positive Definite Band Matrices.* Numerische Mathematik, Vol. 7, 1965, pp. 355-361.

13. Noble, B. — *Applied Linear Algebra.* Prentice-Hall, 1965.

14. Abdelmalek, N.N. — *An Efficient Method for the Discrete Linear L_1 Approximation Problem.* Mathematics of Computation, Vol. 29, 1975, pp. 844-850.

15. Abdelmalek, N.N. — *On the Discrete Linear L_1 Approximation and L_1 Solutions of Overdetermined Linear Equations.* Journal of Approximation Theory, Vol. 11, 1974, pp. 38-53.

16. Abdelmalek, N.N. — *Chebyshev Solution of Overdetermined Systems of Linear Equations.* BIT, Vol. 15, 1975, pp. 117-129.

17. Abdelmalek, N.N. — *A Computer Program for the Chebyshev Solution of Overdetermined Systems of Linear Equations.* Int. J. for Numerical Methods in Engineering, Vol. 10, 1976, pp. 1197-1202.

18. Jacocks, J.L. — *An Investigation of the Aerodynamic Characteristics of Ventilated Test Section Walls for Transonic Wind Tunnels.* Dissertation, The University of Tennessee, December 1976.

19. Kacprzynski, J.J. — *A Method for Calculation of the Linearized Subcritical Flow Past an Arbitrary Airfoil in the Wind Tunnel with Porous Walls.* NRC/NAE Lab Memo HSA-65, National Research Council Canada, Ottawa, Ontario, July 1972.

20. Ebihara, M. — *A Study of Subsonic, Two-Dimensional Wall-Interference Effect in a Perforated Wind Tunnel with Particular Reference to the NAL 2m × 2m Transonic Wind Tunnel.* TR-252T, National Aerospace Laboratory, Japan, January 1972.

21. Mokry, M. — *A Wake-Blockage Paradox in a Perforated Wall Wind Tunnel.* AIAA Journal, Vol. 9, 1971, pp. 2462-2464.

22. Williams, B.R. — *An Exact Test Case for the Plane Potential Flow About Two Adjacent Lifting Aerofoils.* Tech. Report 71197, Royal Aircraft Establishment, September 1971.

23. Choo, D.O. — *An Analysis Method for the Viscous/Inviscid Flow Around Two Dimensional Multi-Element Aerofoils Including Surface Roughness Effects.* Thesis, Carleton University, Ottawa, October 1977.

24. Weibust, E. — *Evaluation of a Computerized Method for Description of the Subsonic, Viscous, Attached Flow About Two-Dimensional, Multi-Component Airfoils.* Tech. Note AU-999, The Aeronautical Research Institute of Sweden, August 1976.

25. Ives, D.C. — *A Modern Look at Conformal Mapping Including Multiply Connected Regions.* AIAA Journal, Vol. 14, 1976, pp. 1006-1011.

26. Nonweiler, T.R.F. — *The Numerical Evaluation of Curvilinear Integrals and Areas.* The Aeronautical Journal of the Royal Aeronautical Soc., Vol. 72, 1968, pp. 887-888.

TABLE 1

EXACT AND COMPUTED PRESSURE COEFFICIENTS FOR THE UNIT CIRCLE, α = 10 DEG.

K	X	Y	CP EXACT	CP L.S.	CP L1	CP L∞
1	1.00000	0.00000	1.00000	1.00000	1.00000	1.00000
2	0.98481	0.17365	0.87939	0.87936	0.87937	0.87936
3	0.93969	0.34202	0.51754	0.51752	0.51754	0.51754
4	0.86603	0.50000	-0.06365	-0.06386	-0.06384	-0.06385
5	0.76604	0.64279	-0.81521	-0.81538	-0.81535	-0.81536
6	0.64279	0.76604	-1.66627	-1.66657	-1.66652	-1.66656
7	0.50000	0.86602	-2.53208	-2.53231	-2.53226	-2.53227
8	0.34202	0.93969	-3.32368	-3.32403	-3.32397	-3.32401
9	0.17365	0.98481	-3.95811	-3.95893	-3.95887	-3.95888
10	0.00000	1.00000	-4.36807	-4.36849	-4.36841	-4.36846
11	-0.17365	0.98481	-4.50980	-4.51067	-4.51060	-4.51062
12	-0.34202	0.93969	-4.36808	-4.36821	-4.36812	-4.36812
13	-0.50000	0.86603	-3.95811	-3.95888	-3.95882	-3.95890
14	-0.64279	0.76605	-3.32368	-3.32448	-3.32443	-3.32446
15	-0.76604	0.64279	-2.53209	-2.53232	-2.53227	-2.53227
16	-0.86602	0.50000	-1.66628	-1.66643	-1.66638	-1.66640
17	-0.93969	0.34202	-0.81521	-0.81537	-0.81534	-0.81537
18	-0.98481	0.17365	-0.06366	-0.06383	-0.06381	-0.06383
19	-1.00000	0.00000	0.51754	0.51751	0.51752	0.51752
20	-0.98481	-0.17365	0.87938	0.87937	0.87938	0.87938
21	-0.93969	-0.34202	1.00000	1.00000	1.00000	1.00000
22	-0.86603	-0.50000	0.88661	0.88659	0.88658	0.88658
23	-0.76605	-0.64279	0.57398	0.57389	0.57387	0.57388
24	-0.64279	-0.76604	0.11964	0.11956	0.11954	0.11955
25	-0.50000	-0.86602	-0.40373	-0.40382	-0.40387	-0.40385
26	-0.34202	-0.93969	-0.91754	-0.91770	-0.91776	-0.91774
27	-0.17365	-0.98481	-1.34729	-1.34769	-1.34777	-1.34774
28	-0.00000	-1.00000	-1.63192	-1.63212	-1.63219	-1.63216
29	0.17365	-0.98481	-1.73143	-1.73187	-1.73194	-1.73194
30	0.34202	-0.93969	-1.63192	-1.63198	-1.63206	-1.63205
31	0.50000	-0.86603	-1.34730	-1.34767	-1.34774	-1.34769
32	0.64279	-0.76605	-0.91755	-0.91790	-0.91795	-0.91791
33	0.76604	-0.64279	-0.40374	-0.40383	-0.40386	-0.40386
34	0.86602	-0.50000	0.11963	0.11958	0.11955	0.11957
35	0.93969	-0.34202	0.57397	0.57393	0.57392	0.57392
36	0.98481	-0.17365	0.88660	0.88658	0.88657	0.88658
37	1.00000	-0.00000	1.00000	1.00000	1.00000	1.00000

TABLE 2

EXACT AND COMPUTED PRESSURE COEFFICIENTS FOR THE KÁRMÁN-TREFFTZ AIRFOIL, α = 0 DEG.

K	X	Y	CP EXACT	CP L.S.	CP L1	CP L∞
1	1.82978	0.00000	1.00000	1.00000	1.00000	1.00000
2	1.79734	0.00669	0.12589	0.16534	0.16561	0.16357
3	1.70471	0.02691	0.04118	0.04757	0.04806	0.04645
4	1.55907	0.05954	-0.04865	-0.03911	-0.03851	-0.03984
5	1.36828	0.10181	-0.14420	-0.13021	-0.12951	-0.13070
6	1.14044	0.14990	-0.24355	-0.22932	-0.22852	-0.22964
7	0.88371	0.19943	-0.34377	-0.33315	-0.33226	-0.33336
8	0.60604	0.24603	-0.44130	-0.43427	-0.43321	-0.43438
9	0.31521	0.28572	-0.53216	-0.52736	-0.52696	-0.52739
10	0.01871	0.31519	-0.61220	-0.60843	-0.60918	-0.60841
11	-0.27623	0.33205	-0.67732	-0.67427	-0.67500	-0.67420
12	-0.56267	0.33491	-0.72358	-0.72100	-0.72147	-0.72090
13	-0.83402	0.32342	-0.74724	-0.74479	-0.74507	-0.74467
14	-1.08406	0.29828	-0.74464	-0.74244	-0.74255	-0.74230
15	-1.30704	0.26110	-0.71139	-0.70899	-0.70898	-0.70885
16	-1.49768	0.21436	-0.64022	-0.63762	-0.63749	-0.63750
17	-1.65128	0.16120	-0.51422	-0.51252	-0.51230	-0.51244
18	-1.76372	0.10521	-0.28281	-0.28675	-0.28643	-0.28671
19	-1.83155	0.05023	0.23061	0.20538	0.20578	0.20536
20	-1.85194	0.00000	1.00000	0.99996	0.99995	0.99996
21	-1.82288	-0.04228	0.17135	0.13566	0.13528	0.13567
22	-1.74358	-0.07412	-0.18487	-0.19570	-0.19598	-0.19559
23	-1.61438	-0.09368	-0.21069	-0.21314	-0.21338	-0.21300
24	-1.43675	-0.10012	-0.15875	-0.16039	-0.16065	-0.16024
25	-1.21347	-0.09383	-0.08660	-0.08814	-0.08846	-0.08799
26	-0.94883	-0.07658	-0.01164	-0.01305	-0.01348	-0.01292
27	-0.64893	-0.05143	0.05900	0.05782	0.05721	0.05793
28	-0.32191	-0.02247	0.12178	0.12093	0.12010	0.12100
29	0.02193	0.00571	0.17470	0.17448	0.17195	0.17451
30	0.37027	0.02872	0.21665	0.21747	0.21975	0.21744
31	0.70921	0.04323	0.24704	0.25003	0.25089	0.24993
32	1.02417	0.04766	0.26563	0.27208	0.27282	0.27188
33	1.30106	0.04261	0.27248	0.28091	0.28154	0.28057
34	1.52761	0.03082	0.26796	0.27415	0.27470	0.27359
35	1.69446	0.01657	0.25306	0.25588	0.25633	0.25494
36	1.79589	0.00478	0.23100	0.24992	0.25019	0.24826
37	1.82978	0.00000	1.00000	1.00000	1.00000	1.00000

TABLE 3

EXACT AND COMPUTED PRESSURE COEFFICIENTS FOR THE KÁRMÁN-TREFFTZ AIRFOIL, α = 0 DEG.

(a) Upper Surface

K	X	Y	CP EXACT	CP L.S.	CP L1	CP L
1	1.82978	0.00000	1.00000	1.00000	1.00000	1.00000
2	1.82150	0.00166	0.16979	0.19699	0.19700	0.19649
3	1.79734	0.00669	0.12589	0.13090	0.13090	0.13062
4	1.75812	0.01514	0.08391	0.08692	0.08694	0.08674
5	1.70471	0.02691	0.04118	0.04565	0.04569	0.04552
6	1.63804	0.04181	-0.00296	0.00296	0.00302	0.00286
7	1.55907	0.05954	-0.04865	-0.04218	-0.04211	-0.04208
8	1.46882	0.07969	-0.09579	-0.08955	-0.08942	-0.08942
9	1.36828	0.10181	-0.14419	-0.13889	-0.13878	-0.13879
10	1.25848	0.12539	-0.19356	-0.18933	-0.18924	-0.18925
11	1.14044	0.14990	-0.24355	-0.24049	-0.24039	-0.24043
12	1.01518	0.17476	-0.29377	-0.29107	-0.29098	-0.29102
13	0.88371	0.19943	-0.34377	-0.34155	-0.34144	-0.34152
14	0.74700	0.22336	-0.39311	-0.39115	-0.39103	-0.39116
15	0.60604	0.24603	-0.44130	-0.43974	-0.43961	-0.43975
16	0.46180	0.26696	-0.48782	-0.48631	-0.48618	-0.48628
17	0.31521	0.28572	-0.53216	-0.53100	-0.53088	-0.53093
18	0.16721	0.30190	-0.57379	-0.57255	-0.57252	-0.57249
19	0.01871	0.31519	-0.61220	-0.61128	-0.61136	-0.61123
20	-0.12940	0.32530	-0.64688	-0.64553	-0.64565	-0.64552
21	-0.27623	0.33205	-0.67732	-0.67673	-0.67684	-0.67673
22	-0.42093	0.33527	-0.70305	-0.70198	-0.70207	-0.70197
23	-0.56267	0.33491	-0.72358	-0.72278	-0.72286	-0.72278
24	-0.70063	0.33094	-0.73846	-0.73770	-0.73776	-0.73768
25	-0.83402	0.32342	-0.74724	-0.74620	-0.74625	-0.74618
26	-0.96208	0.31248	-0.74946	-0.74878	-0.74881	-0.74876
27	-1.08406	0.29828	-0.74464	-0.74366	-0.74368	-0.74363
28	-1.19928	0.28106	-0.73219	-0.73155	-0.73157	-0.73152
29	-1.30704	0.26110	-0.71139	-0.71018	-0.71018	-0.71015
30	-1.40671	0.23875	-0.68124	-0.68068	-0.68067	-0.68064
31	-1.49768	0.21436	-0.64022	-0.63912	-0.63910	-0.63908
32	-1.57938	0.18837	-0.58591	-0.58502	-0.58499	-0.58497
33	-1.65128	0.16120	-0.51423	-0.51349	-0.51346	-0.51344
34	-1.71288	0.13332	-0.41780	-0.41747	-0.41742	-0.41741
35	-1.76372	0.10521	-0.28281	-0.28325	-0.28320	-0.28320
36	-1.80341	0.07735	-0.08253	-0.08539	-0.08534	-0.08533
37	-1.83155	0.05023	0.23061	0.22338	0.22344	0.22357
38	-1.84782	0.02430	0.68687	0.68002	0.68006	0.67990
39	-1.85194	0.00000	1.00000	1.00000	1.00000	1.00000

TABLE 3

EXACT AND COMPUTED PRESSURE COEFFICIENTS FOR THE KÁRMÁN-TREFFTZ AIRFOIL, α = 0 DEG.

(b) Lower Surface

K	X	Y	CP EXACT	CP L.S.	CP L1	CP L
39	-1.85194	0.00000	1.00000	1.00000	1.00000	1.00000
40	-1.84367	-0.02231	0.65458	0.64499	0.64495	0.64502
41	-1.82288	-0.04228	0.17135	0.15979	0.15974	0.15982
42	-1.78952	-0.05964	-0.08265	-0.08858	-0.08864	-0.08855
43	-1.74358	-0.07412	-0.18486	-0.18742	-0.18746	-0.18739
44	-1.68515	-0.08551	-0.21496	-0.21573	-0.21576	-0.21569
45	-1.61438	-0.09368	-0.21069	-0.21134	-0.21136	-0.21129
46	-1.53148	-0.09854	-0.18919	-0.18925	-0.18927	-0.18920
47	-1.43675	-0.10012	-0.15875	-0.15941	-0.15944	-0.15929
48	-1.33059	-0.09848	-0.12372	-0.12374	-0.12378	-0.12383
49	-1.21347	-0.09383	-0.08659	-0.08697	-0.08701	-0.08699
50	-1.08598	-0.08641	-0.04890	-0.04932	-0.04937	-0.04933
51	-0.94883	-0.07658	-0.01164	-0.01197	-0.01203	-0.01198
52	-0.80282	-0.06476	0.02449	0.02404	0.02397	0.02403
53	-0.64893	-0.05143	0.05900	0.05880	0.05871	0.05879
54	-0.48822	-0.03715	0.09152	0.09110	0.09099	0.09110
55	-0.32191	-0.02247	0.12178	0.12169	0.12155	0.12160
56	-0.15137	-0.00800	0.14956	0.14929	0.14910	0.14907
57	0.02193	0.00571	0.17470	0.17467	0.17398	0.17490
58	0.19638	0.01810	0.19709	0.19699	0.19767	0.19706
59	0.37027	0.02872	0.21665	0.21668	0.21687	0.21683
60	0.54182	0.03719	0.23331	0.23360	0.23375	0.23345
61	0.70921	0.04323	0.24704	0.24744	0.24757	0.24727
62	0.87060	0.04672	0.25781	0.25853	0.25865	0.25867
63	1.02417	0.04766	0.26563	0.26673	0.26683	0.26678
64	1.16820	0.04620	0.27051	0.27229	0.27238	0.27235
65	1.30107	0.04261	0.27249	0.27492	0.27502	0.27500
66	1.42129	0.03732	0.27161	0.27518	0.27528	0.27531
67	1.52761	0.03082	0.26796	0.27211	0.27218	0.27228
68	1.61894	0.02370	0.26170	0.26583	0.26589	0.26570
69	1.69446	0.01657	0.25306	0.25602	0.25607	0.25590
70	1.75357	0.01007	0.24249	0.24484	0.24487	0.24467
71	1.79589	0.00478	0.23099	0.23376	0.23377	0.23350
72	1.82129	0.00127	0.22164	0.23938	0.23939	0.23888
73	1.82978	0.00000	1.00000	1.00000	1.00000	1.00000

TABLE 4

EXACT AND COMPUTED PRESSURE COEFFICIENTS FOR THE WILLIAMS' AIRFOIL

(a) Main Airfoil

K	X	Y	CP EXACT	CP L.S.	CPW L.S.	CPF L.S.
1	1.00000	0.00590	1.00000	1.00000	1.00000	1.00000
2	0.99753	0.00718	-0.92119	0.04587	0.10010	0.08039
3	0.99043	0.01041	-1.60169	-1.28191	-1.14999	-1.19640
4	0.97850	0.01458	-1.95374	-1.81638	-1.64768	-1.70556
5	0.96122	0.01893	-1.95727	-1.88111	-1.70060	-1.75970
6	0.93815	0.02323	-1.80900	-1.75887	-1.57704	-1.63325
7	0.90929	0.02762	-1.65810	-1.62122	-1.43827	-1.49139
8	0.87501	0.03232	-1.55225	-1.52459	-1.33714	-1.38770
9	0.83597	0.03743	-1.49342	-1.47106	-1.27514	-1.32483
10	0.79290	0.04293	-1.47265	-1.45337	-1.24534	-1.29462
11	0.74656	0.04870	-1.48106	-1.46572	-1.24185	-1.29149
12	0.69769	0.05453	-1.51204	-1.49832	-1.25516	-1.30503
13	0.64697	0.06020	-1.56109	-1.54760	-1.28176	-1.33289
14	0.59507	0.06550	-1.62525	-1.61339	-1.32087	-1.37364
15	0.54258	0.07019	-1.70272	-1.69087	-1.36771	-1.42234
16	0.49010	0.07408	-1.79260	-1.78096	-1.42255	-1.47939
17	0.43814	0.07700	-1.89477	-1.88299	-1.48396	-1.54353
18	0.38724	0.07881	-2.00992	-1.99672	-1.55112	-1.61352
19	0.33785	0.07942	-2.13965	-2.12720	-1.62717	-1.69285
20	0.29044	0.07875	-2.28674	-2.27347	-1.70994	-1.77848
21	0.24543	0.07678	-2.45564	-2.44087	-1.80202	-1.87456
22	0.20321	0.07352	-2.65315	-2.63538	-1.90580	-1.98304
23	0.16414	0.06902	-2.88974	-2.87138	-2.02934	-2.11143
24	0.12857	0.06335	-3.18166	-3.15722	-2.17355	-2.26326
25	0.09681	0.05663	-3.55471	-3.52746	-2.35716	-2.45386
26	0.06914	0.04898	-4.05084	-4.01407	-2.59032	-2.69696
27	0.04582	0.04056	-4.73940	-4.68560	-2.89974	-3.01957
28	0.02707	0.03155	-5.73037	-5.66525	-3.32930	-3.46787
29	0.01311	0.02211	-7.14534	-7.04428	-3.86413	-4.02814
30	0.00409	0.01242	-8.73166	-8.63074	-4.27026	-4.46058
31	0.00017	0.00264	-8.34989	-8.23135	-3.34768	-3.51898
32	0.00143	-0.00714	-4.20249	-4.06761	-0.85589	-0.94154
33	0.00783	-0.01681	-0.79779	-0.72045	0.62225	0.59881
34	0.01927	-0.02625	0.53705	0.56552	0.98451	0.98185
35	0.03560	-0.03530	0.93296	0.94009	0.96878	0.97028
36	0.05663	-0.04378	0.99969	0.99923	0.86330	0.86379
37	0.08214	-0.05151	0.95724	0.95401	0.75138	0.74943
38	0.11190	-0.05833	0.88385	0.87971	0.65537	0.65056
39	0.14563	-0.06409	0.80830	0.80372	0.57904	0.57188
40	0.18304	-0.06866	0.74118	0.73664	0.52239	0.51316
41	0.22381	-0.07194	0.68596	0.68166	0.48291	0.47187
42	0.26759	-0.07386	0.64327	0.63916	0.45806	0.44578
43	0.31398	-0.07438	0.61252	0.60873	0.44590	0.43259
44	0.36259	-0.07350	0.59271	0.58900	0.44408	0.43018
45	0.41297	-0.07124	0.58264	0.57916	0.45141	0.43711
46	0.46466	-0.06766	0.58115	0.57823	0.46665	0.45218
47	0.51716	-0.06287	0.58708	0.58434	0.48763	0.47344
48	0.56993	-0.05699	0.59936	0.59689	0.51385	0.50008
49	0.62240	-0.05018	0.61699	0.61473	0.54409	0.53090
50	0.67396	-0.04261	0.63898	0.63732	0.57794	0.56555
51	0.72396	-0.03451	0.66437	0.66310	0.61382	0.60234
52	0.77169	-0.02612	0.69205	0.69122	0.65101	0.64060
53	0.81639	-0.01771	0.72058	0.72072	0.68873	0.67941
54	0.85728	-0.00965	0.74766	0.74876	0.72417	0.71605
55	0.89358	-0.00236	0.76914	0.77198	0.75422	0.74712
56	0.92461	0.00361	0.77689	0.78302	0.77172	0.76538
57	0.94998	0.00766	0.75477	0.76694	0.76243	0.75621
58	0.96975	0.00941	0.67369	0.69919	0.70342	0.69619
59	0.98434	0.00903	0.50061	0.56694	0.58296	0.57362
60	0.99417	0.00748	0.23687	0.53967	0.56155	0.55217
61	0.99931	0.00612	-0.04022	0.92122	0.92522	0.92342
62	1.00000	0.00590	1.00000	1.00000	1.00000	1.00000

TABLE 4

EXACT AND COMPUTED PRESSURE COEFFICIENTS FOR THE WILLIAMS' AIRFOIL

(b) Flap

K	X	Y	CP EXACT	CP L.S.	CPW L.S.	CPF L.S.
63	1.31389	-0.20363	1.00000	1.00000	1.00000	1.00000
64	1.31303	-0.20226	0.48483	0.76958	0.76388	0.75787
65	1.31064	-0.19840	0.35456	0.46537	0.45447	0.43889
66	1.30697	-0.19245	0.21788	0.27382	0.26245	0.24102
67	1.30214	-0.18476	0.06777	0.10545	0.09498	0.06910
68	1.29624	-0.17566	-0.09789	-0.06624	-0.07421	-0.10467
69	1.28934	-0.16544	-0.27961	-0.25439	-0.25897	-0.29446
70	1.28147	-0.15440	-0.47687	-0.45517	-0.45494	-0.49494
71	1.27267	-0.14281	-0.68829	-0.66691	-0.66044	-0.70553
72	1.26298	-0.13090	-0.91168	-0.89182	-0.87759	-0.92841
73	1.25245	-0.11891	-1.14405	-1.12698	-1.10344	-1.15865
74	1.24112	-0.10704	-1.38159	-1.36371	-1.32944	-1.38963
75	1.22907	-0.09548	-1.61970	-1.60314	-1.55672	-1.62158
76	1.21637	-0.08439	-1.85307	-1.83794	-1.77787	-1.84776
77	1.20310	-0.07391	-2.07571	-2.05802	-1.98368	-2.05725
78	1.18938	-0.06416	-2.28112	-2.26795	-2.17825	-2.25574
79	1.17532	-0.05525	-2.46235	-2.45054	-2.34563	-2.42601
80	1.16103	-0.04725	-2.61232	-2.59494	-2.47541	-2.55762
81	1.14667	-0.04020	-2.72396	-2.71844	-2.58451	-2.66871
82	1.13235	-0.03415	-2.79067	-2.77975	-2.63385	-2.71859
83	1.11824	-0.02909	-2.80664	-2.79715	-2.64193	-2.72534
84	1.10447	-0.02499	-2.76751	-2.76340	-2.60035	-2.68258
85	1.09119	-0.02181	-2.67093	-2.66599	-2.49944	-2.57950
86	1.07852	-0.01946	-2.51744	-2.51908	-2.35279	-2.42920
87	1.06658	-0.01785	-2.31124	-2.30997	-2.14791	-2.21890
88	1.05548	-0.01684	-2.06103	-2.07179	-1.91663	-1.98175
89	1.04527	-0.01631	-1.78052	-1.78872	-1.64433	-1.70380
90	1.03600	-0.01610	-1.48844	-1.49669	-1.36490	-1.41779
91	1.02768	-0.01606	-1.20757	-1.22866	-1.10884	-1.15597
92	1.02027	-0.01609	-0.96299	-0.97432	-0.86664	-0.90815
93	1.01372	-0.01607	-0.77990	-0.80112	-0.70139	-0.73857
94	1.00797	-0.01598	-0.68332	-0.69789	-0.60189	-0.63752
95	1.00295	-0.01582	-0.70367	-0.72929	-0.62914	-0.66421
96	0.99864	-0.01569	-0.89891	-0.91783	-0.80164	-0.84029
97	0.99508	-0.01571	-1.43049	-1.43817	-1.27849	-1.32822
98	0.99242	-0.01604	-2.85918	-2.90141	-2.61311	-2.68891
99	0.99087	-0.01686	-5.75997	-5.58808	-4.98532	-5.10521
100	0.99073	-0.01835	-1.17476	-1.14602	-0.87380	-0.90639
101	0.99226	-0.02065	0.71658	0.72756	0.78574	0.78340
102	0.99572	-0.02381	0.98154	0.98088	0.99118	0.99142
103	1.00134	-0.02781	0.99520	0.99579	0.98955	0.98883
104	1.00930	-0.03258	0.96308	0.96461	0.95093	0.94876
105	1.01972	-0.03807	0.92597	0.92760	0.91000	0.90651
106	1.03263	-0.04423	0.89341	0.89482	0.87506	0.87055
107	1.04799	-0.05105	0.86722	0.86810	0.84726	0.84189
108	1.06565	-0.05854	0.84699	0.84748	0.82626	0.82037
109	1.08535	-0.06674	0.83159	0.83185	0.81076	0.80430
110	1.10676	-0.07572	0.81976	0.81967	0.79900	0.79232
111	1.12944	-0.08553	0.81022	0.81013	0.79013	0.78309
112	1.15285	-0.09619	0.80184	0.80166	0.78237	0.77521
113	1.17640	-0.10766	0.79358	0.79344	0.77490	0.76746
114	1.19948	-0.11982	0.78457	0.78453	0.76669	0.75899
115	1.22146	-0.13243	0.77401	0.77439	0.75719	0.74924
116	1.24177	-0.14518	0.76122	0.76168	0.74501	0.73669
117	1.25995	-0.15765	0.74560	0.74705	0.73086	0.72204
118	1.27564	-0.16939	0.72668	0.72965	0.71391	0.70481
119	1.28864	-0.17996	0.70420	0.70980	0.69457	0.68494
120	1.29886	-0.18893	0.67827	0.69020	0.67548	0.66543
121	1.30635	-0.19598	0.64997	0.67854	0.66485	0.65459
122	1.31121	-0.20083	0.62318	0.72813	0.71747	0.70939
123	1.31360	-0.20335	0.61683	0.92443	0.92156	0.91993
124	1.31389	-0.20363	1.00000	1.00000	1.00000	1.00000

TABLE 5

EXACT AND COMPUTED FORCE COEFFICIENTS FOR THE WILLIAMS' AIRFOIL IN FREE AIR, α = 0 DEG.

Lift Force Coefficients

	Main Airfoil	Flap	Total
Exact	2.1853	0.6242	2.8095
Source Panel	2.1579	0.6003	2.7582
Vortex Panel	2.1662	0.6225	2.7887

Drag Force Coefficients

	Main Airfoil	Flap	Total
Exact	-0.2886	0.2886	0.0000
Source Panel	-0.2821	0.2676	-0.0145
Vortex Panel	-0.2861	0.2867	0.0006

TABLE 6

COMPUTED FORCE COEFFICIENTS FOR THE WILLIAMS' AIRFOIL IN THE WIND TUNNEL AND FREE AIR, BY THE VORTEX PANEL METHOD

Lift Force Coefficients

	Main Airfoil	Flap	Total
Wind Tunnel ($\alpha = 0.000°$)	1.6906	0.5949	2.2854
Free Air ($\alpha = -3.958°$)	1.7200	0.6268	2.3468
Wind Tunnel Corrected for $\Delta\alpha = -3.958°$	1.6783	0.6127	2.2910

Drag Force Coefficients

	Main Airfoil	Flap	Total
Wind Tunnel ($\alpha = 0.000°$)	-0.1187	0.2785	0.1598
Free Air ($\alpha = -3.958°$)	-0.2433	0.2426	-0.0007
Wind Tunnel Corrected for $\Delta\alpha = -3.958°$	-0.2351	0.2367	0.0016

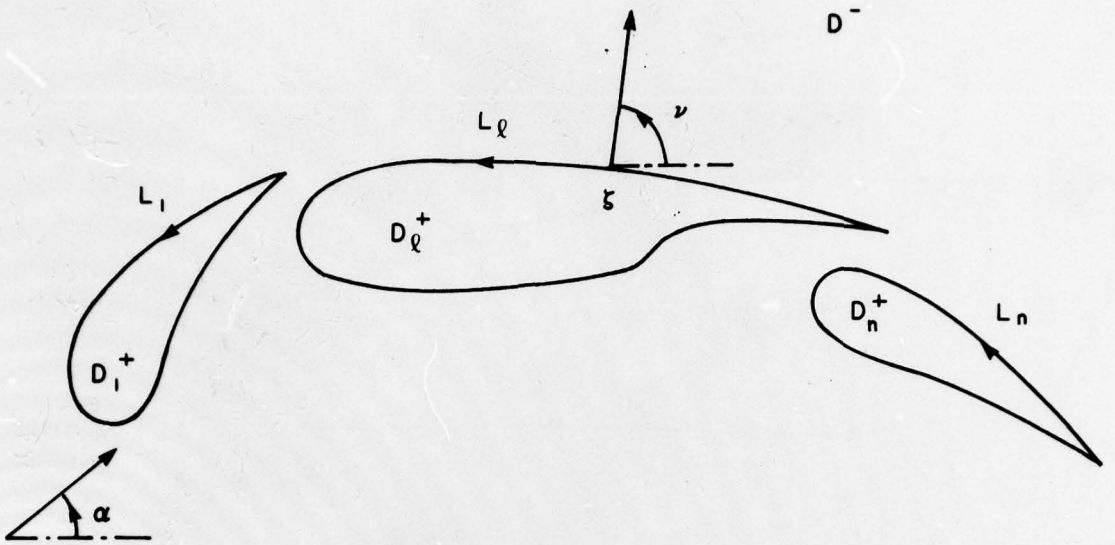

FIG. 1: MULTIPLY CONNECTED FLOW REGION

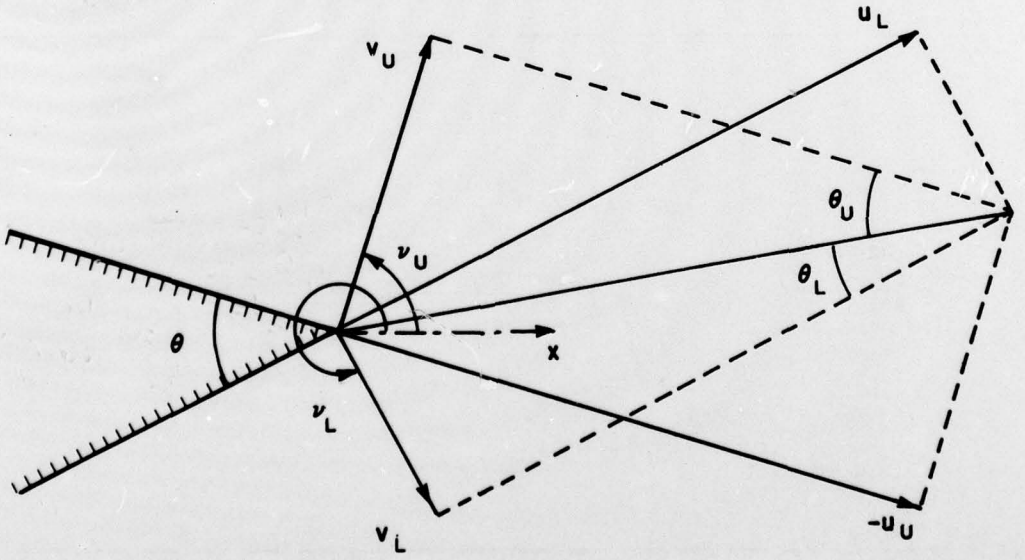

FIG. 2: TRAILING EDGE VELOCITIES

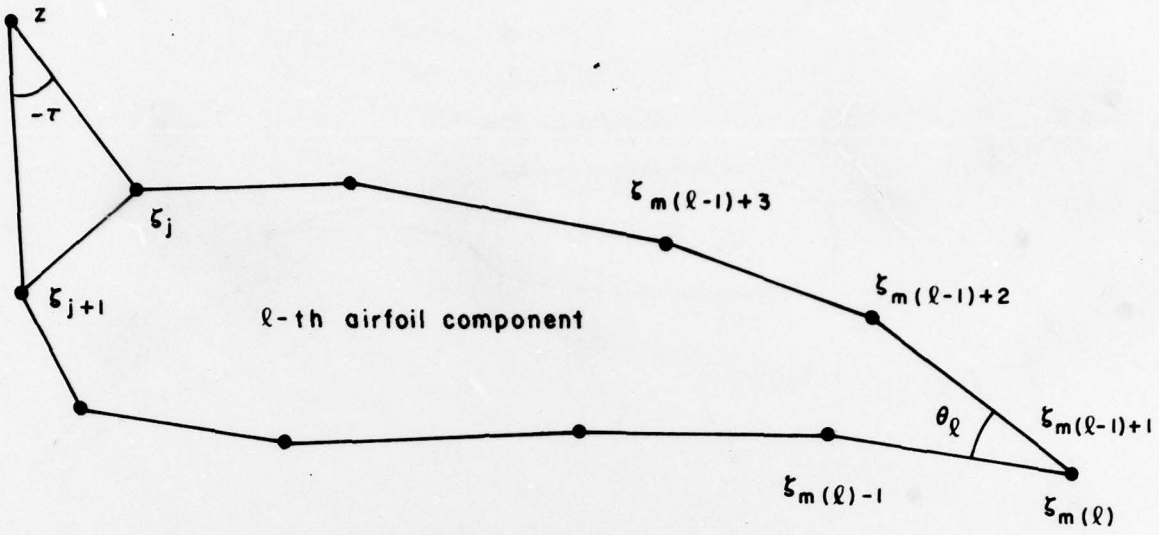

FIG. 3: AIRFOIL COMPONENT REPRESENTED BY AN INSCRIBED POLYGON

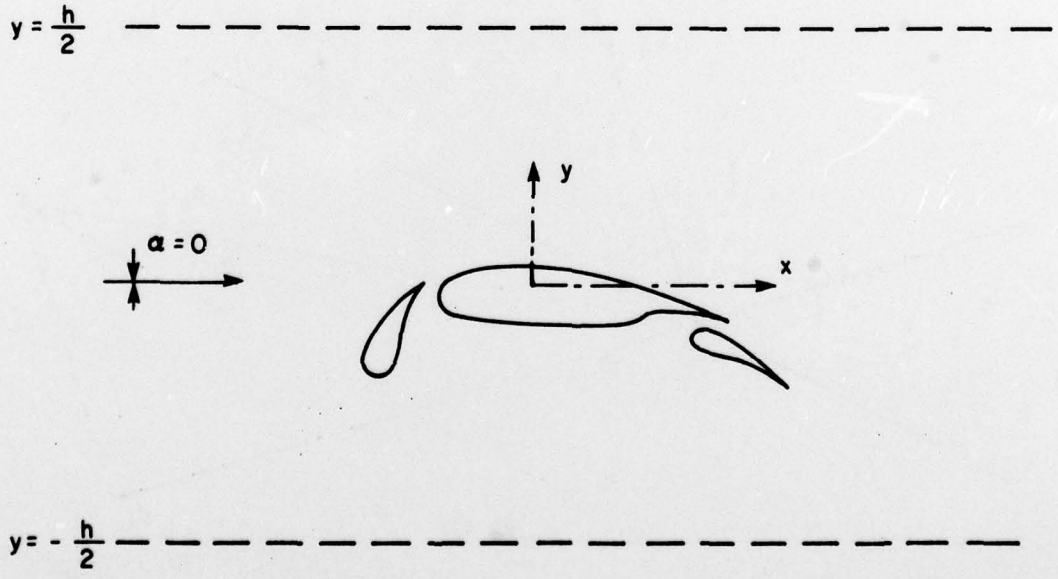

FIG. 4: WIND TUNNEL CO-ORDINATE SYSTEM

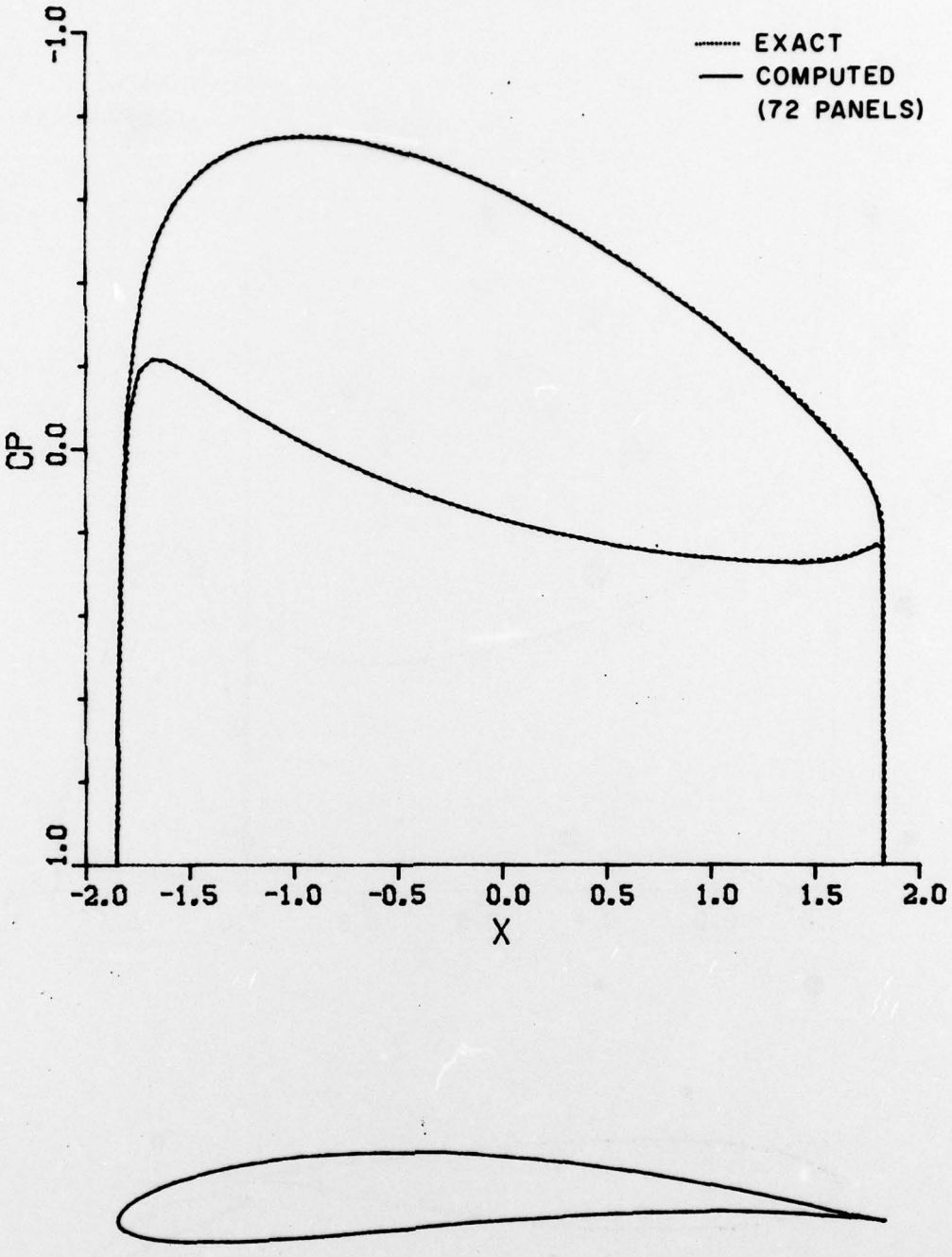

FIG. 5: EXACT AND COMPUTED PRESSURE DISTRIBUTIONS ON THE KÁRMÁN-TREFFTZ AIRFOIL, $\alpha = 0$ DEG.

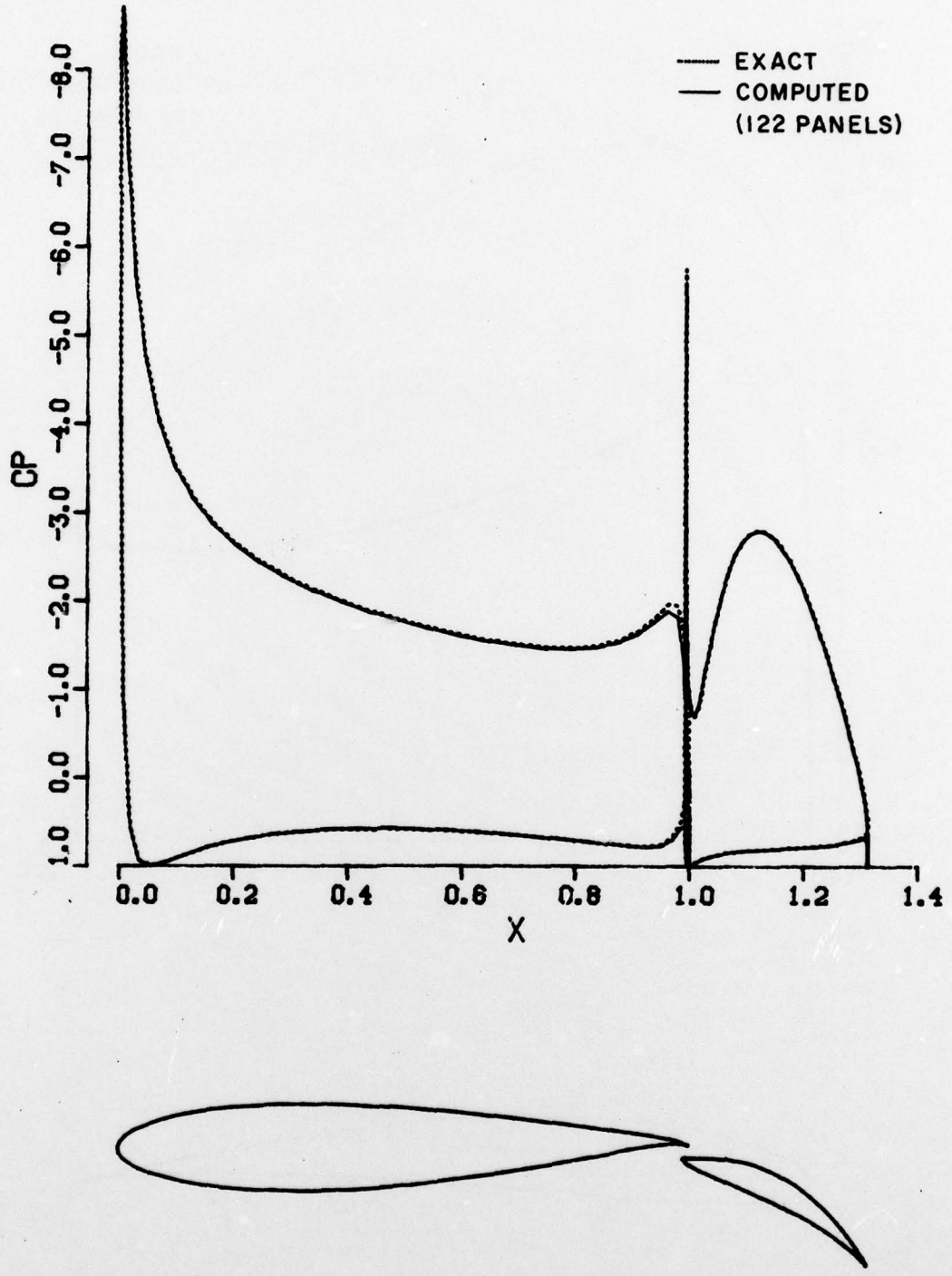

FIG. 6: EXACT AND COMPUTED PRESSURE DISTRIBUTIONS ON THE WILLIAMS' AIRFOIL, α = 0 DEG.

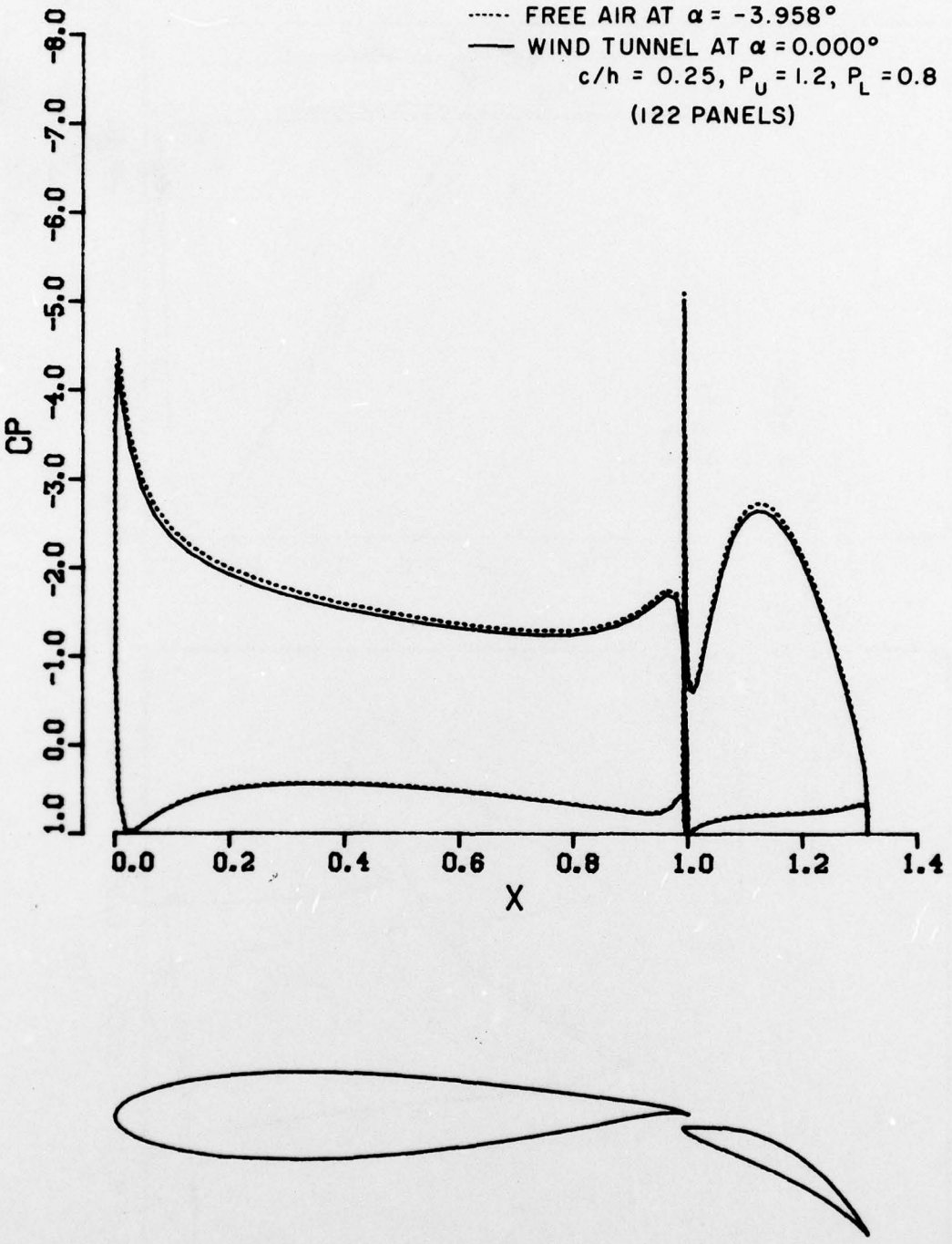

FIG. 7: PRESSURE DISTRIBUTIONS COMPUTED FOR THE WILLIAMS' AIRFOIL IN FREE AIR AND IN THE WIND TUNNEL

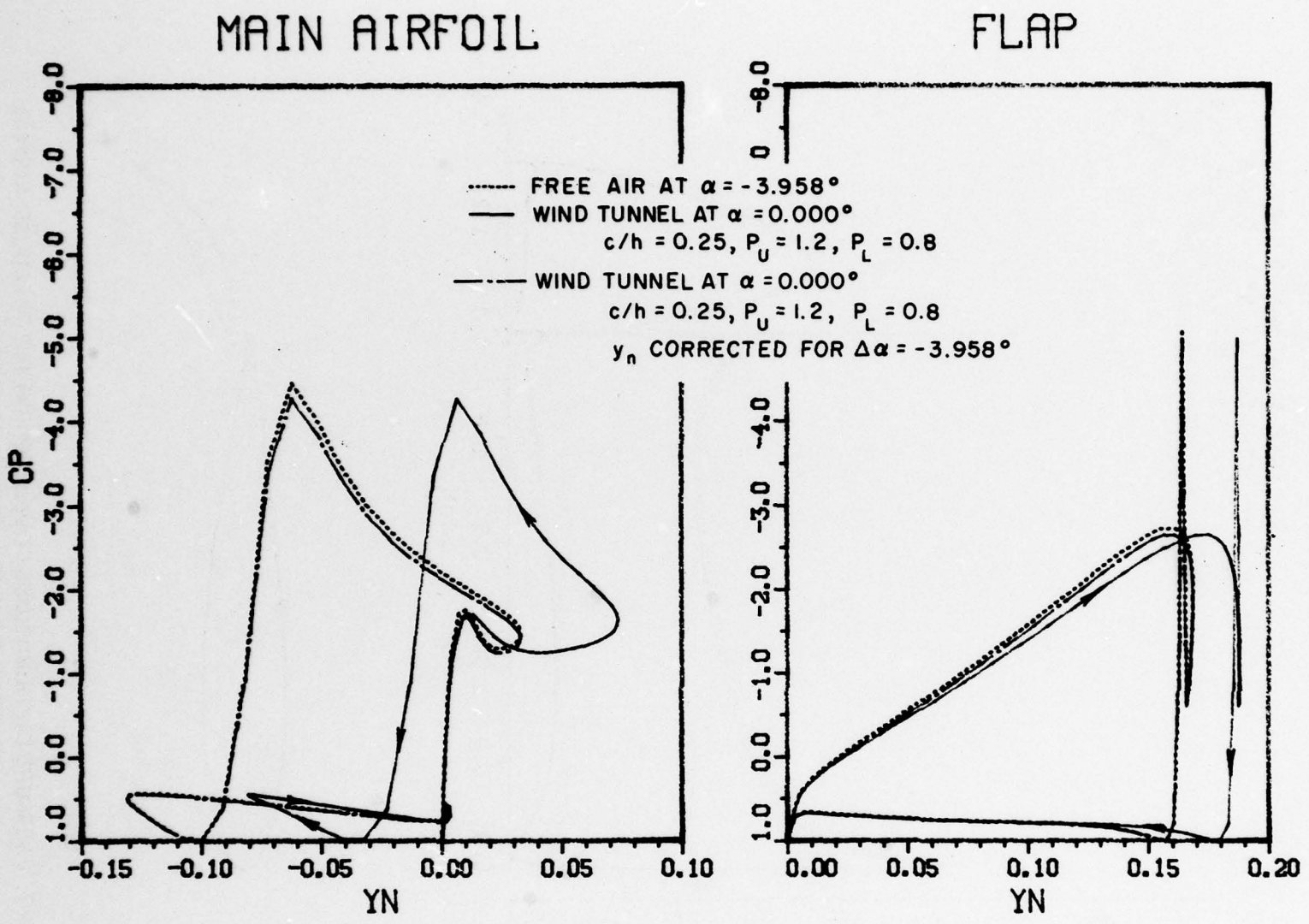

FIG. 8: DRAG LOOPS COMPUTED FOR THE WILLIAMS' AIRFOIL IN FREE AIR AND IN THE WIND TUNNEL

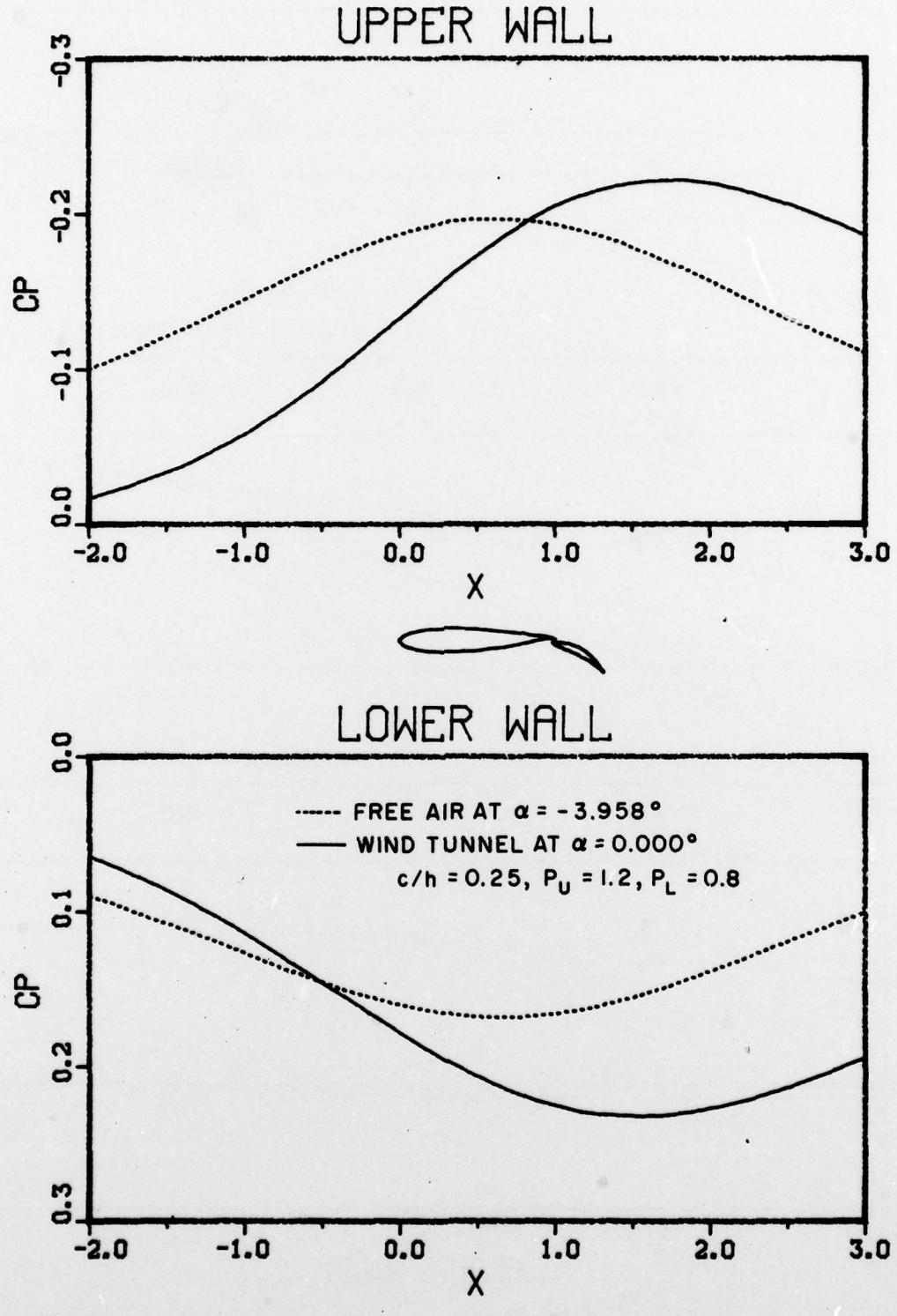

FIG. 9: PRESSURE DISTRIBUTIONS AT THE LOCATION OF THE WALLS, COMPUTED FOR THE WILLIAMS' AIRFOIL IN FREE AIR AND IN THE WIND TUNNEL

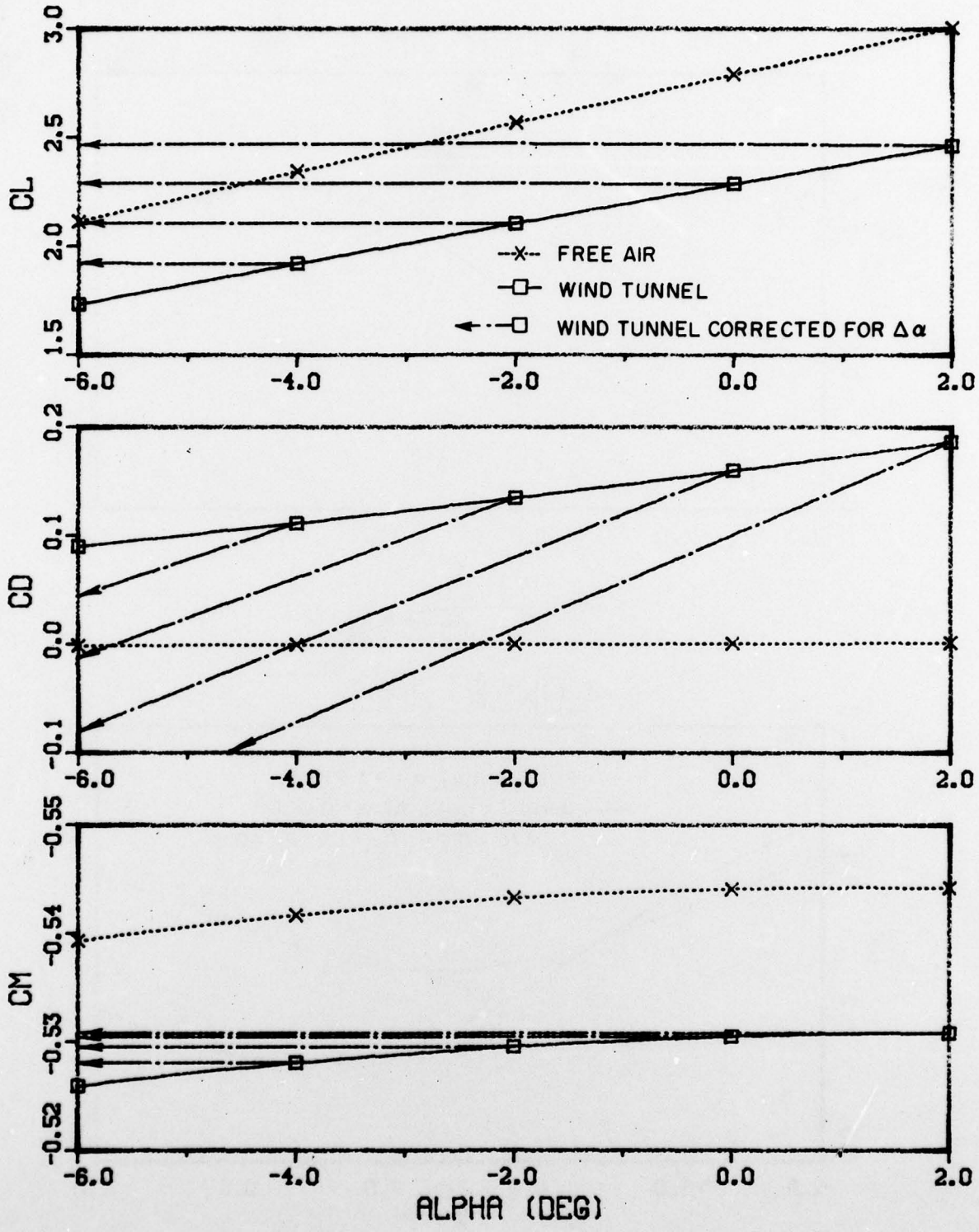

FIG. 10: LIFT FORCE, DRAG FORCE, AND QUARTER-CHORD PITCHING MOMENT COEFFICIENTS COMPUTED FOR THE WILLIAMS' AIRFOIL IN FREE AIR AND IN THE WIND TUNNEL

NRC, NAE LR-596
National Research Council Canada. National Aeronautical Establishment.

CALCULATION OF THE POTENTIAL FLOW PAST MULTI-COMPONENT AIRFOILS USING A VORTEX PANEL METHOD IN THE COMPLEX PLANE.
Mokry, M. November 1978. 49 pp. (incl. tables and figures).

An efficient algorithm for a vortex panel method in the complex plane is developed to compute the potential flow past multi-component airfoils in free air and a porous-wall wind tunnel. The theoretical foundations of the method — the properties of the source and vortex density functions, the relationship between the exterior and interior flows, and the general Kutta-Joukowski condition for a trailing edge with crossflow — are derived from the theory of the Cauchy type integral. The method utilizes flat panels with linear vortex and source densities, the latter being used to simulate the displacement effect of boundary layers. The airfoil boundary condition is satisfied at all panel midpoints and the overdetermined system of linear algebraic equations solved as a least squares problem, in the L_1 norm, or in the L_∞ norm. The wind tunnel wall interference problem is treated using the concept of the Green's function in the complex plane. Examples are worked out for some theoretical airfoils and extensive tables of exact and computed pressure distributions are given.

UNCLASSIFIED

1. Potential flow.
2. Vortices.
3. Panels.

I. Mokry, M.
II. NRC, NAE LR-596

NRC No. 17246

NRC, NAE LR-596
National Research Council Canada. National Aeronautical Establishment.

CALCULATION OF THE POTENTIAL FLOW PAST MULTI-COMPONENT AIRFOILS USING A VORTEX PANEL METHOD IN THE COMPLEX PLANE.
Mokry, M. November 1978. 49 pp. (incl. tables and figures).

An efficient algorithm for a vortex panel method in the complex plane is developed to compute the potential flow past multi-component airfoils in free air and a porous-wall wind tunnel. The theoretical foundations of the method — the properties of the source and vortex density functions, the relationship between the exterior and interior flows, and the general Kutta-Joukowski condition for a trailing edge with crossflow — are derived from the theory of the Cauchy type integral. The method utilizes flat panels with linear vortex and source densities, the latter being used to simulate the displacement effect of boundary layers. The airfoil boundary condition is satisfied at all panel midpoints and the overdetermined system of linear algebraic equations solved as a least squares problem, in the L_1 norm, or in the L_∞ norm. The wind tunnel wall interference problem is treated using the concept of the Green's function in the complex plane. Examples are worked out for some theoretical airfoils and extensive tables of exact and computed pressure distributions are given.

UNCLASSIFIED

1. Potential flow.
2. Vortices.
3. Panels.

I. Mokry, M.
II. NRC, NAE LR-596

NRC No. 17246

NRC, NAE LR-596
National Research Council Canada. National Aeronautical Establishment.

CALCULATION OF THE POTENTIAL FLOW PAST MULTI-COMPONENT AIRFOILS USING A VORTEX PANEL METHOD IN THE COMPLEX PLANE.
Mokry, M. November 1978. 49 pp. (incl. tables and figures).

An efficient algorithm for a vortex panel method in the complex plane is developed to compute the potential flow past multi-component airfoils in free air and a porous-wall wind tunnel. The theoretical foundations of the method — the properties of the source and vortex density functions, the relationship between the exterior and interior flows, and the general Kutta-Joukowski condition for a trailing edge with crossflow — are derived from the theory of the Cauchy type integral. The method utilizes flat panels with linear vortex and source densities, the latter being used to simulate the displacement effect of boundary layers. The airfoil boundary condition is satisfied at all panel midpoints and the overdetermined system of linear algebraic equations solved as a least squares problem, in the L_1 norm, or in the L_∞ norm. The wind tunnel wall interference problem is treated using the concept of the Green's function in the complex plane. Examples are worked out for some theoretical airfoils and extensive tables of exact and computed pressure distributions are given.

UNCLASSIFIED

1. Potential flow.
2. Vortices.
3. Panels.

I. Mokry, M.
II. NRC, NAE LR-596

NRC No. 17246

NRC, NAE LR-596
National Research Council Canada. National Aeronautical Establishment.

CALCULATION OF THE POTENTIAL FLOW PAST MULTI-COMPONENT AIRFOILS USING A VORTEX PANEL METHOD IN THE COMPLEX PLANE.
Mokry, M. November 1978. 49 pp. (incl. tables and figures).

An efficient algorithm for a vortex panel method in the complex plane is developed to compute the potential flow past multi-component airfoils in free air and a porous-wall wind tunnel. The theoretical foundations of the method — the properties of the source and vortex density functions, the relationship between the exterior and interior flows, and the general Kutta-Joukowski condition for a trailing edge with crossflow — are derived from the theory of the Cauchy type integral. The method utilizes flat panels with linear vortex and source densities, the latter being used to simulate the displacement effect of boundary layers. The airfoil boundary condition is satisfied at all panel midpoints and the overdetermined system of linear algebraic equations solved as a least squares problem, in the L_1 norm, or in the L_∞ norm. The wind tunnel wall interference problem is treated using the concept of the Green's function in the complex plane. Examples are worked out for some theoretical airfoils and extensive tables of exact and computed pressure distributions are given.

UNCLASSIFIED

1. Potential flow.
2. Vortices.
3. Panels.

I. Mokry, M.
II. NRC, NAE LR-596

NRC No. 17246